RADIATION SHIELDING PROPERTIES OF FIVE CLAY BRICKS

A Dissertation

Submitted to the 'Dean Office, Institute of Science & Technology' in the Partial Fulfillment for the Requirement of Master's Degree of Science in Physics

By

Birendra Khadka

Exam Roll No.: PHY 3563/076

T.U. Regd. No.: 5-2-0061-0037-2015

November 12, 2024

Recommendation

It is certified that **Mr. Birendra Khadka** has carried out the dissertation entitled **"RADIATION SHIELDING PROPERTIES OF FIVE CLAY BRICKS "** under our supervision. We recommend the dissertation in the partial fulfillment of the requirement of Master's Degree of Science in Physics.

.....

(Supervisor)
Dr. Raju Khanal
Professor
Central Department of Physics
Tribhuvan University
Kathmandu, Nepal

.....

(Co-Supervisor)
Mr. Devendra Raj Upadhyay
Lecturer
Department of Physics, Amrit Campus
Tribhuvan University
Kathmandu, Nepal

Acknowledgement

I am thankful to Supervisor Prof. Dr. Raju Khanal, Central Department of Physics, Tribhuvan University, and Co-Supervisor Mr. Devendra Raj Upadhyay, Lecturer of Physics, Amrit Campus, Tribhuvan University for helping in all steps and guiding on this dissertation work. I am thankful to the Head of Department of Physics Dr. Janak Ratna Malla, Amrit Campus, Thamel, Kathmandu also gratitude towards M.Sc. Physics coordinator and lecturer of Amrit Campus, Mr. Pitamber Shrestha, for providing platform and motivating in dissertation work.

I am thankful to the Ministry of Industry, Tourism, Forest and Environment of Dhangadhi, Kailali, which has provided financial support for this research work.

I would like to thank the Ministry of Education, Science and Technology, Government of Nepal, and the International Atomic Energy Agency (IAEA) for their support in setting up the Nuclear Research Laboratory at the Central Department of Physics, Tribhuvan University, Kirtipur (through TC project NEP0002) and Ministry of Education, Science and Technology, Government of Nepal (for coordination with IAEA).

Last but not least, I would like to sincerely thank all those who contributed and encouraged me to complete this project. I thank everyone who gave me the motivation I needed to finish my dissertation. I would especially like to acknowledge the contributions of Uddab Bahadur Bhandari and Gaurab Koirala. I am so grateful to my mother for her support and motivation.

Evaluation

We certify that we have read this dissertation work entitled **"RADIATION SHIELDING PROPERTIES OF FIVE CLAY BRICKS"**. In our opinion, it qualifies in the scope and quality as dissertation in partial fulfillment for the requirement of Master's Degree of Science in Physics.

Evaluation Committee

.....

(Supervisor)
Dr. Raju Khanal
Professor
Central Department of Physics
Tribhuvan University

.....

(Co-Supervisor)
Mr. Devendra Raj Upadhyay
Lecturer
Department of Physics
Amrit Campus
Tribhuvan University

.....

Assoc. Prof. Dr. Janak Ratna Malla
Head of Department
Department of Physics
Amrit Campus
Tribhuvan University
Kathmandu, Nepal

.....

Asst. Prof. Pitamber Shrestha
M.Sc. Coordinator
Department of Physics
Amrit Campus
Tribhuvan University
Kathmandu, Nepal

.....

Internal

.....

External

Sep. 6, 2024

Abstract

The use of radioactive materials in power generation, medical research, industry and agriculture research is essential to the scientific and economic advancement of a nation. Different ionizing radiation has the potential to seriously harm human health as well as the environment. The main goal of a radiation shield is to minimize the radiation emitted by an emitter to a level that is acceptable in the area outside the shield, while taking into consideration the possible risks of ionizing radiation exposure. The radiation shielding properties of five brick brand samples named as Newa, Harati, Hira, KTM and PK from different construction sites of the Kathmandu valley are analyzed by using photon shielding and dosimetry (Phy-X/PSD) software within the energy of 15 keV to 15 MeV. The mass attenuation coefficients (*MAC*), linear attenuation coefficient (*LAC*) were theoretically calculated using the elemental compositions of the bricks provided by the inductively coupled plasma optical emission spectrometry (ICP-OES). Elemental analysis technique as input data for PhyX/PSD software. The highest *MAC* values is obtained at low energy 15 keV in the order of 122.52 cm^2 g^{-1} to 67.37 cm^2 g^{-1} lowest *MAC* values is obtained at high energy 15 MeV in order of 1.02×10^{-2} cm^2 g^{-1} to 1.85 $\times10^{-2}$ cm^2 g^{-1}. The highest *HVL* value ranges from 21.45 cm to 43.09 cm within the energy range of 15 keV to 15 MeV and the lowest *HVL* value ranges from 0.33×10^{-2} cm to 0.66×10^{-2} cm. Smaller the value of *HVL*, *TVL* and *MFP* more will be the photon attenuation capacity. The maximum effective atomic number Z_{eff} is 16.36 for the Harati brand brick sample. The lowest value of Z_{eff} is 14.75 for Newa brand brick. Whole obtained data depicts that among the studied five bricks Hira brand brick sample is best for shielding and PK brand brick has least shielding among five selected samples.

Keywords: Radiation Shielding, ICP-OES, Phy-X/PSD software, attenuation coefficient

शोधसार

विकिरणले मानव स्वास्थ्यमा गम्भीर असर पुऱ्याउन सक्छ। विशेष गरी मेडिकल क्षेत्र, परमाणु ऊर्जा र औद्योगिक क्षेत्रमा विकिरणबाट सुरक्षा आवश्यक छ। ईटा, ढुङ्गा जस्ता निर्माणका साधनले हानिकारक विकिरणलाई रोक्न वा न्यून गर्न सहयोग पुऱ्याउँछ। नेपालमा हस्पिटलहरूमा एक्स–रे, सिटी स्क्यान जस्ता उपकरणहरूको प्रयोग हुने गरेको छ र त्यस्ता उपकरणबाट निस्किने विकिरण रोक्न विकिरण अवरोधकको आवश्यकता हुन्छ जसले स्वास्थ्यकर्मी र बिरामीलाई सुरक्षा प्रदान गर्छ। रेडियोधर्मी पदार्थहरूको सुरक्षित भण्डारण, त्यसको निरिक्षण, र यसको प्रयोगपछि सुरक्षित रूपमा नष्ट गर्न आवश्यक हुन्छ। ईटाले रेडियोधर्मी पदार्थबाट निस्केका विकिरणबाट सुरक्षा प्रदान गर्न सक्छ कि सक्दैन र ति रेडियोधर्मी पदार्थको भण्डारण गर्न साकिन्छ कि भनेर काठमाडौं उपत्यकाका विभिन्न निर्माणस्थलबाट नेवा, हारति, हिरा, केटीएम र पिके नामक भिन्नाभिन्नै ब्राण्डका पाँचवटा ईटा नमूनाहरूको विकिरण अवरोध गुणहरू PhyX/PSD को प्रयोग गरेर विश्लेषण गरियो। PhyX/PSD सफ्टवेयरको गामा रे शक्ति १५ keV देखि १५ MeV थियो। ICP–OES द्वारा ईटाको रसायनिक तत्व को रचना थाहा पाइयो। ईटामा भयका तत्व हरुलाई PhyX/PSD सफ्टवेयरमा इनपुट तथ्याङ्कको रूपमा प्रयोग गरि रेखिय विकिरण रोक्ने गुणांक LAC, पिण्डले विकिरण रोक्ने गुणांक MAC, विकिरणको शक्ति आधा पार्ने तह HVL, विकिरणको शक्ति नब्बे प्रतिशतले घटाउने तह TVL, वस्तुको प्रभावकारि परमाणु संख्या Z_{eff}, वस्तुको प्रभावकारी चालकता C_{eff}, वस्तुको प्रभावकारी ईलेक्ट्रोन घनत्व N_{eff}, द्रुत न्यूट्रॉनको टक्कर हुने सम्भावना $FNRCS$ को विश्लेषण गरियो। जसबाट हिरा ब्राण्ड ईटाको उच्चतम विकिरण प्रतिरोधक गुण र पिके ब्राण्ड ईटाको कम विकिरण प्रतिरोधक गुण पाइयो। सबै भन्दा बढि MAC को मान हिरा ब्राण्ड ईटाको पाइयो जुन मान १२२.५2 वर्ग से.मी प्रति ग्राम र कम MAC मान केटिएम ईटामा पाइयो जुन ६७.३७ वर्ग से.मी प्रति ग्राम छ । त्यसैगरी LAC को उच्चतम मान हिरा ईटाको पाइयो जुन २१३.१८ प्रति से.मि. र न्युनतम मान पिके ईटामा पाइयो जुन १०५.७७ प्रति से.मि. प्राप्त गरियो । त्यसैगरी HVL को उच्चतममान पिके ब्राण्डको ईटामा पाइयो जुन ४३.०९ से.मि. र न्युनतम मान हिरा ब्राण्डको ईटामा पाइयो जुन २१.४५ से.मि. प्राप्त गरियो । Z_{eff} को उच्चतम मान हारति ईटा मा पाइयो जुन १६.३६ र न्युनतम मान नेवा ईटामा १४.७५ प्राप्त गरियो । MFP को उच्चतम मान पिके ईटामा पाइयो जुन ६२.१७ से.मि. पाइयो र न्युनतम मान ३०.९५ से.मि. प्राप्त गरियो। सम्पूर्ण प्राप्त तथ्याङ्कको विश्लेसण गर्दा अध्ययन गरिएका पाँचवटा ईटामध्ये हिरा ईटाको रेडियोधर्मी विकिरण प्रतिरोध गुण सबैभन्दा उत्तम पाइयो भने पिके ईटाको रेडियोधर्मी विकिरण प्रतिरोध गर्ने क्षमता कम भएको पाइयो ।

Acronyms and Abbreviations

ACS Atomic Cross Section.

C_{eff} Effective Conductivity.

EABF Energy Absorption Builtup Factor.

EBF Energy Builtup Factor.

FNRCS Fast Neutron Removable Cross Section.

HVL Half Value Layer.

LAC Linear Attenuation Coefficient.

MAC Mass Attenuation Coefficient.

MFP Mean Free Path.

N_{eff} Effective Electron Density.

TVL Tenth Value Layer.

Z_{eff} Effective Atomic Number.

ANN Artificial Neutral Network.

GEP Gene Expression Programming.

ICP-OES Inductively Coupled Plasma-Optical Emission Spectrometry.

ns Nanosecond.

Pb Lead.

PHITS Particle and Heavy Ion Transport Code System.

Phy-X/PSD Phy-X/Photon Shielding and Dosimetry.

RSFs Radiation Shielding Films.

S m^{-1} siemens per meter.

List of Figures

List of Tables

Contents

Chapter 1

Introduction

The radiation leak disasters at Fukushima, Japan (2011) and Chernobyl, Ukraine (1986) highlighted the critical necessity for methodological and exact research on the robustness and efficiency of construction materials employed as radiation shields. The use of radioactive materials in power generation, medical, industry and agricultural research is essential to a nation's scientific and economic advancement. Nuclear technology has several major applications, such as the detection and treatment of various diseases, electricity generation, environmental control and archaeology. Different radioactive rays, including gamma rays, X-rays and neutrons, are used in nuclear technology and have the potential to seriously harm human health as well as the environment. The main goal of a radiation shield is to minimize the radiation emitted by an emitter to a level acceptable in the area outside the shield while taking into account the possible risks of exposure to ionizing radiation [1].

Clay has been found to have good refractory qualities, including a high melting point, thermochemical stability, good mechanical strength at high temperature, low thermal shrinkage, great resistance to corrosion and high thermal shock resistance [2]. Clay is a composite material that is widely accessible, making it an eco-friendly, economical and non-poisonous substance [3]. Clay materials are deemed acceptable for consideration in shielding applications because to these qualities.

Due to numerous disadvantages, traditional shielding materials like Pb, concrete and depleted uranium have been progressively restricted. For example, there are problems with Pb and Pb-based compounds. In light of the growing number of fields that use radiation-emitting devices

and radioactive isotopes, it is essential to investigate the gamma-ray shielding capacity of easily accessible building materials such as clay [4]. Fascinatingly, clay is a widely accessible composite material that is economical, nontoxic and environmentally friendly. Because of these characteristics, clay materials are a good option to consider for shielding.

In the context of Nepal, most of the houses are made up of bricks and use cement mortar. It is important to study the effectiveness of bricks over radiation shielding. For this purpose, five brick brand samples were collected from five different construction sites in the Kathmandu valley and analyzed for different parameters of radiation shielding.

1.1 Background

Radiation

Radiation is the term for energy that permeates the atmosphere and manifests itself as particles or waves. In addition to radioactive materials found in food, water, soil, air and the human body. People can be exposed to radiation via cosmic rays. In industry, academia and medical, human-made radiation sources are commonly used. Radiation can be classified as either non-ionizing or ionizing [5]. The different types of radiation and their penetration strength against different types of barriers are shown in Figure 1.1 [6].

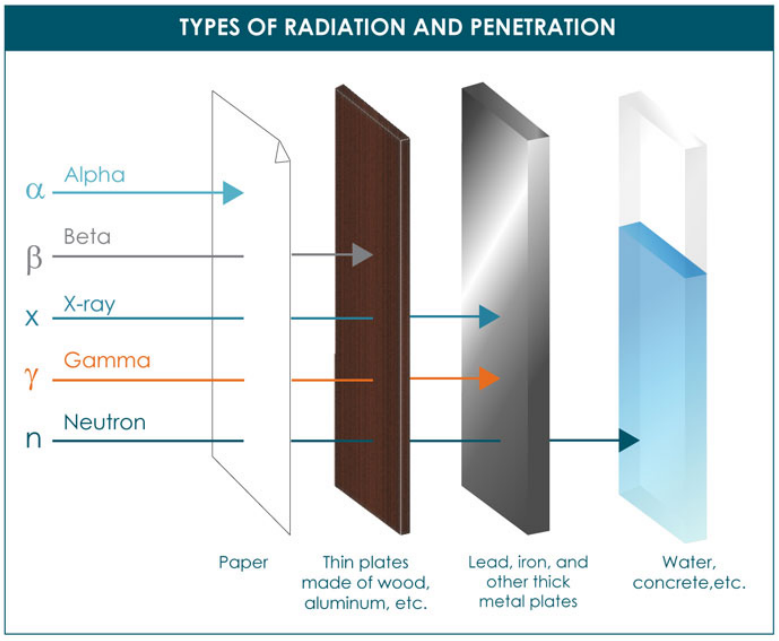

Figure 1.1: Types of barriers and penetrating strength of radiations.

Non ionization radiation

Non-ionizing radiation is defined as radiation where there is insufficient energy to produce ionization. It is composed of visible, ultraviolet and infrared light, as well as radio waves, microwaves, electric and magnetic fields and optical radiation [7].

Both naturally occurring and intentionally manufactured electromagnetic field sources fall under the category of non-ionizing radiation. Appliances and electrical power supplies are the most common producers of low-frequency electric and magnetic fields in our living areas. Radio frequency electromagnetic fields are frequently produced by microwave ovens, television antennas and telecommunication equipment [8].

Ionization radiation

Ionizing radiation as radiation that has enough energy to remove tightly bound electrons from atoms, creating ions. This process can cause chemical changes in cells that can cause damage to living tissue. Ionizing radiation includes particles such as alpha and beta particles, as well as electromagnetic radiation such as gamma rays and X-rays. Ionizing radiation is significant in various fields, including medicine, industry and research. Although it is beneficial in applications such as cancer treatment and medical imaging, it can also pose health risks if not properly managed [8].

The production of nuclear power and many other industrial and research applications use artificial radiation sources; however, the majority of human exposure to ionizing radiation nowadays comes from medical applications (e.g. diagnostic radiology, image-guided interventions, nuclear medicine and radiotherapy) [9].

Ionizing radiation takes a few forms: α, β, γ, neutron particles and X-rays. All types of radiation are caused by an unstable nucleus. In order to reach a stable state, they must release energy or mass in the form of radiation [5].

Radioactive decay and the resulting radiation

Unstable nuclei that release energy when they change to more stable states can be the source of ionizing radiation. When an unstable nucleus decays, ionizing radiation is emitted, such as β, γ and neutron particles. Proper handling and storage of this radiation can have several beneficial outcomes [5].

Most common types of radioactive decay

Ionizing radiation arises from radioactive decay processes, influenced by the type of particles or waves the nucleus emits to stabilize.

Alpha radiation:

Alpha decay is possible whenever the mass of the original parent isotope (unstable nucleus) is greater than the sum of the masses of the final daughter nucleus (stable nucleus) and a neutral ${}^{4}_{2}\mathrm{He}$ nucleus as shown in Eq. (1.1). Alpha particles are emitted at high speeds, typically a few percent of the speed of light. Despite this, alpha particles can travel only a few centimeters in air or a few tenths or hundredths of a millimeter through solids because of their mass and charge before colliding and coming to rest. Heavy, positively charged particles are released by decaying nuclei in alpha radiation as a means of gaining stability. In many cases, the use of just one sheet of paper can prevent these particles from harming us because they cannot penetrate our skin [5].

$$\underset{\mathrm{Parent-isotope}}{{}^{A}_{Z}\mathrm{X}} \rightarrow \underset{\alpha-\mathrm{particle}}{{}^{4}_{2}\mathrm{He}} + \underset{\mathrm{Daughter-isotope}}{{}^{A-4}_{Z-2}\mathrm{Y}} \tag{1.1}$$

However, ingestion, breathing or drinking alpha-emitting substances can be directly exposed to tissues, which could be harmful to health [7].

Beta radiation

Beta-minus decay or electron emission: Degradation can occur when the mass of the final nucleus is lower than that of the initial neutral nucleus.

$$n \rightarrow p + \beta^{-} + \bar{\nu}_{e} \tag{1.2}$$

Beta-plus decay or positron emission: Anytime the mass of the initial neutral nucleus is at least two electron masses greater than the mass of the end nucleus, decay can take place as shown in Eq. (1.3).

$$p \rightarrow n + \beta^{+} + \nu_{e} \tag{1.3}$$

Electron capture: It can happen if the end nuclues mass is less than the original neutral nucleus mass as shown in Eq. (1.4) [5].

$$\mathrm{p} + \beta^{-} \rightarrow \mathrm{n} + \nu_e \tag{1.4}$$

Gamma radiation

Gamma radiation is a form of electromagnetic radiation with high energy and short wavelength, typically emitted by radioactive substances during nuclear decay processes. It is highly penetrating and can pass through most materials, making it useful in medical imaging and cancer treatment, but also requires careful shielding to protect against its harmful effects [10].

Neutrons

By colliding with nuclei or being absorbed by them, neutrons indirectly produce ionization, which is then followed by radioactive decay of the resultant nuclei. One of the main components of the nucleus is the neutrons, which are relatively heavy particles. Because they are uncharged, they cannot directly cause ionization. However, X-ray, gamma, beta and alpha radiation may be produced via their interactions with the atoms of matter, leading to ionization. Neutrons cannot be stopped; they can only be stopped with dense amounts of concrete, water, or paraffin [5].

X-ray

X-rays are a type of electromagnetic radiation that have wavelengths that are longer than ultraviolet light and shorter than gamma rays. They are produced when high-energy electrons strike a metal target or when electrons within an atom shift in energy. X-rays are widely used in medical imaging because of their ability to penetrate tissues and produce images of the inside of the body, particularly for the identification of fractures and other internal structures [11].

Neutron radiation

Free neutrons, which are typically released as a consequence of induced or spontaneous nuclear fission, make up neutron radiation. Though they can travel hundreds or even thousands of meters in the air, they can be efficiently stopped if they come into contact with a substance that is rich in hydrogen, such water or concrete. Since they absorb into stable atoms, neutrons are typically indirectly ionizing, increasing the likelihood that the stable atom may emit another form of ionizing radiation. This is due to the fact that neutrons often lack a charge, which prevents them from directly ionizing an atom. Neutron radiation is actually the sole kind of radiation that has the ability to radioactively alter other things [12].

Radioactive isotope

A radioactive isotope also known as a radionuclide, is an atom with an unstable nucleus that decays over time and emits radiation in the form of beta, gamma, or alpha rays. This decay process converts the isotope into a new element or a more stable isotope of the parent element. Radioactive isotopes have applications in science, medicine and business, such as tracking chemical reactions, radiometric dating and cancer treatment [13].

1.2 Radiation shielding

The process of using materials to absorb or stop the passage of ionizing and non-ionizing radiation is known as radiation shielding. Depending on the kind and energy of radiation involved, lead, concrete and specialty polymers are often used materials for radiation shielding. In nuclear, industrial and medical settings, effective shielding is essential to prevent radiation exposure and ensure worker safety [14]. Ionizing radiation shielding material is any material that absorbs or filters damaging radiation emitted by radiating sources and protects against it. The concept of radiation shielding was developed to protect itself from the harmful effects of radiation. Hospital, radiotherapy, nuclear laboratories, spaceships, aircraft and nuclear energy power plants are all examples where individuals are directly exposed to hazardous radiation. Glass has been examined because it is chemically inert, thermally stable and most importantly transparent. Phosphate glasses offer a wide range of uses due to their unique properties, which include a low melting point, low refractive indices, low optical dispersion indices, high transparency and a high thermal expansion coefficient [15]. Burnt clay bricks have moderate gamma ray shielding abilities, while clay bricks show comparatively superior shielding behavior [16].

1.3 Interaction of radiation with matter

When radiation interacts with materials, a variety of events take place, including ionization, scattering and absorption. Since radiation imparts energy to atoms and molecules, it has the power to excite or ionize matter. This interaction is determined by the properties of the material and the kind of radiation (alpha, beta and gamma). An understanding of these interactions is crucial in fields including radiation therapy, medical imaging and radiation protection [17].

Photoelectric effect

The photoelectric effect is a phenomenon in which electrons are ejected from the surface of a material when it is exposed to light of sufficient energy. This effect was first observed by Heinrich Hertz in 1887 and later explained by Albert Einstein in 1905, who proposed that light consists of particles called photons. Each photon carries a quantum of energy and when this energy is greater than the work function of the material, it can dislodge electrons from the surface. Einstein's explanation of the photoelectric effect provided strong evidence for the quantum nature of light and earned him the Nobel Prize in Physics in 1921 [18].

When a material absorbs radiation, the photoelectric effect transfers all of the energy from the gamma ray to an electron in the inner shell of the atom. This leads to the complete disappearance of the gamma photon and the ejection of an electron with an energy equal to the gamma photon's starting energy minus the electron's binding energy. The energy of the interacting gamma photon is substantially higher than this binding energy. The events in a detector material can then be caused by the released electron. When an electron from another shell moves into the electron gap in the inner shell, an X-ray photon is produced [19]. The equation of the photoelectric effect is given by Einstein's photoelectric equation in Eq. (1.5).

$$E = h\nu = \phi + \text{K. E.} \tag{1.5}$$

where:

- E is the energy of the incoming photon.
- h is Planck's constant (6.63×10^{-34} J s).
- ν is the frequency of the light that enters.
- ϕ is the work function of the material (the minimum energy required to remove an electron from the surface of the material).
- K.E. is the kinetic energy of the electron emitted.

Rearranging this equation, we get:

$$\text{K.E.} = h\nu - \phi \tag{1.6}$$

This shows that the kinetic energy of the emitted electrons depends on the frequency of the

incident light and the work function of the material. If the energy of the incoming photons is greater than the work function, electrons will be emitted and the excess energy will be converted into the kinetic energy of these electrons as shown in Figure 1.2 [20].

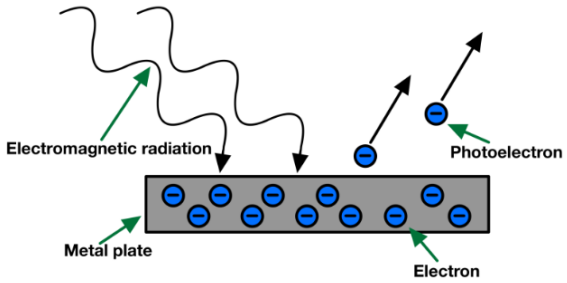

Figure 1.2: Schematic diagram of Photoelectric effect.

1.4 Photoelectric absorption

When an incident photon interacts with the atom during photoelectric absorption, an electron is released from one of the inner shells of the atom. This phenomenon is most noticeable at photon energies that are just a little higher than the electron's binding energy in its shell. Because photoelectric absorption is highly dependent on the atomic number of the material, it is essential for radiation shielding and X-ray imaging applications [21].

Compton effect

Compton Scattering, another name for the Compton Effect, is a basic physics phenomena that explains how electrons scatter high-energy photons, such as gamma or X-rays. When Arthur Compton made the discovery in 1923, it offered compelling proof that light behaves like a particle.

In this process, an electron receives a portion of the energy and momentum that a high-energy photon imparts to it upon collision. The photon changes in wavelength (or energy) as a result of this impact because it scatters at an angle that differs from its initial direction as shown in Figure 1.3. The angle of scattering determines how much momentum and energy are delivered to the electron [22].

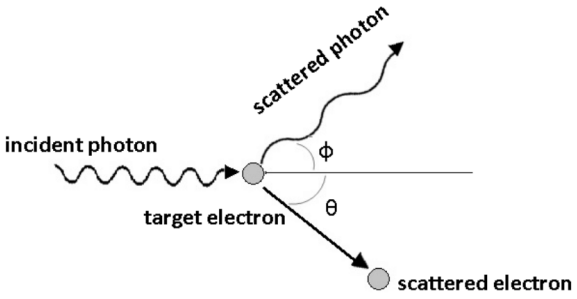

Figure 1.3: Schematic diagram of Compton effect.

The equation of the Compton effect is given by Eq. (1.7).

$$\Delta\lambda = \lambda' - \lambda = \frac{h}{m_e c}(1 - \cos\theta) \tag{1.7}$$

where:

- $\Delta\lambda$ is the change in wavelength.
- λ is the initial wavelength of the photon.
- λ' is the wavelength of the scattered photon.
- h is Planck's constant (6.63×10^{-34} J s).
- m_e is the rest mass of the electron (9.11×10^{-31} kg).
- c is the speed of light in a vacuum (3×10^{8} m s^{-1}).
- θ is the scattering angle of the photon.

1.5 Compton scattering

When an incident X-ray or gamma photon collides with a loosely bound electron, a phenomenon known as Compton scattering occurs. This energy transfer results in the photon scattering at a lower energy (longer wavelength) and the electron recoiling. This phenomenon is frequently used in many domains, including particle physics, astrophysics and medical imaging and is important in understanding the dual nature of light [23].

Pair production

A gamma-ray photon, a high-energy photon, interacts with a nucleus or other particle to produce

a pair of particles-antiparticles. This process is known as pair creation and is a fundamental one in particle physics. Einstein's equation E=mc^2, which allows energy (E) to be converted into mass (m) and vice versa, governs this process [24].

Pair production is a quantum phenomenon in which a γ-ray photon, with sufficient energy, is converted into an electron-positron pair when it interacts with the electromagnetic field of a nucleus or an electron as shown in Figure 1.4. The energy requirement for pair production is given by Eq. (1.8).

$$E_\gamma \geq 2m_e c^2 \tag{1.8}$$

where:

- E_γ is the energy of the gamma-ray photon.
- m_e is the rest mass of the electron (and positron), 9.11×10^{-31} kg.
- c is the speed of light in a vacuum, 3×10^8 m s^{-1}.

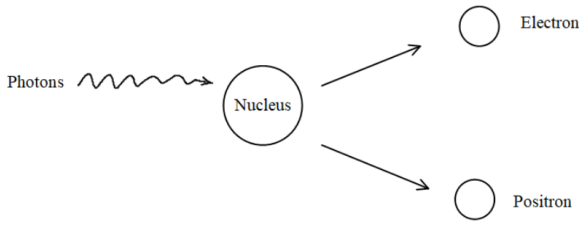

Figure 1.4: Schematic diagram of Pair Production.

Triple production

When three charged leptons, such as taus, muons and electrons are produced simultaneously in high-energy collisions or interactions, it is known as triplet formation. It aids in the study of particle interactions and characteristics at extremely high energies, allowing physicists to gain understanding of the basic basis of forces and matter [25]. Triplet production is a process where a high-energy photon interacts with an atomic electron, producing an electron-positron pair while the original electron remains free. The energy requirement for triplet production is given by the Eq. (1.9).

$$E_\gamma \geq 4m_e c^2 \tag{1.9}$$

where:

- E_γ is the energy of the incoming photon.
- m_e is the rest mass of the electron (and positron), 9.11×10^{-31} kg.
- c is the speed of light in a vacuum, 3×10^8 m s^{-1}.

Bremsstrahlung

The term "braking radiation," or "bremsstrahlung," in German, describes the electromagnetic radiation released when an electron or other charged particle slows down or changes direction as a result of interactions with matter or other charged particles. Depending on the particle energy involved, this radiation can occur at a wide variety of frequencies, from radio waves to X-rays. It is essentially the radiation that is created during "braking" or deceleration of a charged particle [26].

Bremsstrahlung, or "braking radiation," is radiation produced by the deceleration of a charged particle, such as an electron, when it is deflected by another charged particle, typically an atomic nucleus. The power radiated by Bremsstrahlung can be described by the following formula in the case of non-relativistic speeds as in Eq.(1.10)

$$P = \frac{e^2 a^2}{6\pi\epsilon_0 c^3} \tag{1.10}$$

where:

- P is the power radiated.
- e is the charge of the electron (1.60×10^{-19} C).
- a is the acceleration of the electron.
- ϵ_0 is the permittivity of free space (8.85×10^{-12} F m^{-1}).
- c is the speed of light in a vacuum (3×10^8 m s^{-1}).

Bethe formula Bethe formula is used in physics to determine how much energy a charged particle like an electron or a proton loses when it travels through a substance. Provides an estimate of the energy that the particle loses per unit length in the material by taking into account a number of elements, including the particle's charge, velocity and the characteristics of the substance through which it is traversing [27].

The Bethe formula for stopping power (energy loss per unit of path length) is given by Eq.

(1.11).

$$-\frac{dE}{dx} = \frac{4\pi z^2 e^4}{m_e c^2 \beta^2}\left(\frac{nZ}{A}\right)\left[\ln\left(\frac{2m_e c^2 \beta^2 \gamma^2 T_{max}}{I^2}\right) - 2\beta^2\right] \tag{1.11}$$

Where:

- $-\frac{dE}{dx}$ is the stopping power.
- z is the charge of the incident particle.
- e is the elementary charge (1.60×10^{-19} C).
- m_e is the rest mass of the electron (9.11×10^{-31} kg).
- c is the speed of light in a vacuum (3×10^8 m s^{-1}).
- $\beta = \frac{v}{c}$ is the velocity of the particle relative to the speed of light.
- $\gamma = \frac{1}{\sqrt{1-\beta^2}}$ is the Lorentz factor.
- n is the electron density of the medium.
- Z is the atomic number of the medium.
- A is the atomic mass of the medium.
- T_{max} represents the highest K that can be transmitted to an electron in free energy during a single collision.
- I is the mean excitation potential of the medium.

1.6 Effect of radiation

X-rays and γ-rays interact with matter through the photoelectric effect, where an electron absorbs a photon and is ejected from its position, or through Compton scattering. Neutrons, however, lead to ionization indirectly, either by colliding with nuclei or being absorbed by them, followed by radioactive decay of the resulting nuclei. These interactions are very intricate. It is widely recognized that excessive radiation exposure, including sunlight, X-rays and nuclear radiation, can cause tissue damage. In mild cases, this manifests as burns, such as sunburn. However, higher levels of exposure can cause severe disease or death through various mechanisms, including extensive tissue cell destruction, genetic mutations and destruction of components of the bone marrow that produce red blood cells [5].

Chapter 2

Literature Review

Radiation shielding is an important aspect in the nuclear electrical energy production, space, hospital and industries, where effective cost-friendly materials are needed to protect against harmful ionizing radiation. Traditional materials such as lead and concrete have been extensively studied and used. However, the investigation and search for more sustainable and cost-effective materials has led researchers to explore natural materials like clay bricks. Some of the study in radiation shielding are as:

Obaid et al.(2017) focused on the importance of rocks and concrete bricks on radiation shielding. WinXCOM programs are used to calculate attenuation coefficients and photon cross sections for various elements and compounds. The effective atomic number is a critical parameter for understanding the attenuation of gamma rays in composite materials. The paper discusses how N_{eff} varies with energy and its implications for medical radiation dosimetry and imaging applications. The mass attenuation coefficient $(\frac{\mu}{\rho})$, the Z_{eff} and the electron density (N_{eff}) are measured for rock and concrete at a gamma-ray energy of 122, 356, 511, 662, 1275, 1330 keV using a NaI (Tl) scintillation detector and *MAC* card [28].

Olukotun et al.(2018) looked into the radiation shielding capacity of two clay materials from southern western Nigeria, Ball clay and Kaolin, for the mass attenuation coefficient $(\frac{\mu}{\rho})$ at photon energies of 609.31 keV - 1764.50 keV emitted from the source ^{214} Bi and ^{60} Co. Clay materials' elemental compositions as determined by gamma-ray transmission and particle-induced X-ray emission experiments were monitored with a hyper pure germanium (HPGe) spectrometer detector. The outcome demonstrates that clay materials can be used for nuclear and medical

gamma radiation shielding [4].

Olarinoye et al.(2020) investigated the gamma-ray interaction parameter (*MAC*, *LAC*, *HVL*, *MFP*, Z_{eff}, Z_{eq}, *EABF*, *EBF* and *FNRCS*) on semiconductor glasses Tellurium oxide (TeO_2)–Vanadium oxide (V_2O_5)–Molybdenum oxide (MoO_3) (TVM_{20}-TVM_{60}) by utilizing WinXcom and EXABCal computer codes. The mechanical characteristics, α particles, γ-ray, proton and neutron interaction parameters of semiconductor glasses ranging from TMV_{20} to TMV_{80} have been examined. For TVM-glasses, the total ionic packing density (V_t) and total dissociation energy (G_t) have been calculated. It has been reported that shielding characteristics and elastic moduli are correlated. Compared to the other glasses, TVM_{60} is found to have a superior fast neutron shielding capacity. Olarinoye et al. suggested TVM_{20}-TVM_{60} glasses are less effective in attenuating photons than TVM_{60} glass (2020) [29].

The usefulness of clay, silica fume and cement samples for radiation shielding were studied by Akbulut et al.(2015). They found that, due to barriers' ability to lessen radiation intensity, shielding is the most effective way to defend against radiation dangers. Investigation found that using of nanoscale oxide to clay minerals improve the efficiency of shielding [30].

Thuong et al.(2024) compared the gamma-ray shielding properties of the newly fabricated white clay-based bricks. The findings suggest that the Vietnam's fabricated bricks exhibit good shielding capacity, indicating their potential for practical applications in radiation protection. The study examined the impact of pressure rate on the shielding qualities, both physical and γ-ray. The NaI (Tl) detector measures the linear attenuation coefficients of the produced bricks throughout an energy range of 0.66 MeV to 1.33 MeV. A decrease in porosity and an increase in density of the bricks improve these coefficients. The bricks' radiation protection efficiency is increased by 10.22%, 14.48%, 14.09% and 14.26% for gamma ray energies of 0.66 MeV, 1.17 MeV, 1.25 MeV and 1.33 MeV, respectively, due to the enhancement in the linear attenuation coefficient [31].

Nzivulu et al.(2024) investigated the potential of waste glass and red clay composites as ionizing radiation shields. The GEANT4 tools and the web-based NIST-XCOM photon attenuation database were used to perform Monte-Carlo simulation. Findings shows that half value layer decreases with increase percent of waste glasses [32].

Bantan et al.(2020) studied rock sample of Egypt experimentally and by using Monte Carlo

simulation and Phy-X/PSD software for calculating mass attenuation coefficient (*MAC*), energy builtup factor (*EBF*), effective atomic number Z_{eff} and energy absorption builtup factor (*EABF*). This study suggest that linear attenuation factor (*LAC*) μ decreases as the photon energy increases [33].

Sayyed et al.(2017) studied the application of Lambert's Beer law in radiation shielding. The energy absorption and exposure buildup factor are vital for evaluating the effectiveness of shielding materials against gamma radiation. This includes findings on mass attenuation coefficients, which were calculated using both theoretical and simulated methods (WinXcom and MCNPX). The *EABF* and *EBF* values are influenced by the equivalent atomic number (Z_{eq}) of the brick [34].

Dulal et al.(2024) examined the attenuation characteristics of silver tellurite glasses against ions, neutrons and gamma rays. In order to simulate and compute different shielding parameters, the study uses sophisticated computational tools including the Particle and Heavy Ion Transport code System (PHITS) Monte Carlo method and theoretical software like Phy-X/PSD and NIST XCOM. They have also estimate effective atomic number, effective electron density and energy absorption build-up factors. They studied photoelectric effect, pair production, Compton scattering and triple production region in the energy range from 1 keV to 100 GeV are some of the ways that radiation interacts with glass materials [35].

El-Saway et al.(2024) studied the gamma-ray shielding parameters for different epoxy composites(especially epoxy resins), polymeric materials. The MCNP-X code is used for simulating radiation interactions with materials when modeling radiation dynamics. They uses artificial neural networks (ANN) to forecast radiation shielding parameters highlights its superiority over traditional techniques [36].

Sayyed et al.(2024) explored glass samples with fixed ratio of PbO to Na_2O and a variable ratio of BaO to B_2O_3 for gamma radiation shielding. They obtained that high-energy electromagnetic radiation poses biological risks, including Deoxyribonucleic Acid (DNA) damage and potential carcinogenesis. The addition of heavy metal oxides to borosilicate glass can significantly enhance ability to attenuate gamma radiation [37].

The effect of the substitution of Ag_2O / V_2O_5 on the radiation shielding ability of a tellurite glass system studied by Olarinoye et al.(2021). They have compared different glass systems,

including those with WO_3 and Bi_2O_3, have shown notable enhancements in shielding against gamma radiation. The investigation employs XCOM and simulations (FLUKA code) to analyze the radiation interaction parameters of the proposed glass systems [38].

Sing et al.(2016) invitation on clay-flyash bricks, which are made from locally sourced clay and flyash collected from thermal power stations. They uses various analytical techniques, including energy-dispersive X-ray spectroscopy (EDX) and X-ray fluorescence, to determine the elemental composition of the clay-flyash bricks. According to the study's findings, a biological shield against low-energy gamma rays can be created using clay-flyash brick exterior walls because to their high absorption efficiency in the event of a nuclear disaster [39].

Kim et al.(2019) investigated the relationship between the porosity during mixing and the preservation of the properties of the shielding film. Porosity is identified as a critical factor that affects the mechanical properties and shielding effectiveness of radiation shielding films RSFs. They found that porosity directly influences the tensile strength and overall shielding performances [40]. Mann et al.(2016) studied the clay bricks for the storage facilities of radioactive waste. They compared fly ash and red mud bricks, burned clay bricks. A number of interaction parameters, including the mass attenuation coefficient, half value layer and effective electron density, are evaluated . They analyzes the chemical compositions of brick samples using wavelength-dispersive X-ray fluorescence (WDXRD) and X-ray diffraction (XRD), as well as theoretical calculations using a modified toolbox for gamma ray interaction coefficients [16].

Amin et al.(2022) found that the density and thickness of a material can affect the ability of radiation shielding. They highlights how artificial neutral networks (ANN) and gene expression programming (GEP) are becoming increasingly important in forecasting a material's ability to protect radiation. ANN models outperform GEP models in terms of accuracy. The investigation demonstrated a high degree of agreement between the expected and experimental outcomes, demonstrating the usefulness of these models for upcoming uses [41].

2.1 Research gap and motivation

Clay exhibits high melting point, thermo-chemical stability, high mechanical strength, resistance to thermal shock, minimal thermal shrinkage and high corrosion resistance. Fascinatingly, clay is a composite material that is economical, nontoxic and ecologically benign. Clay

materials have these qualities, which make them suitable for use as shields.

In Nepal, bricks made of burned clay are used to build most buildings. There is no standard measures for manufacturing wall width for radiation shielding at public levels.

Every day, more and more nuclear weapons and power plants are being deployed around the world. This investigation was motivated by the need for an emergency response plan, the opportunity to broaden the body of scientific knowledge and the requirement to provide practical data that would help analysts in their work.

2.2 Objectives

The following are our objectives, which are divided into two parts they are:

General Objective

To investigate the radiation shielding efficiencies of clay bricks.

Specific Objectives

1. To estimate chemical composition of the clay bricks.
2. To analyze gamma radiation shielding parameters such as mass attenuation coefficient (*MAC*), linear attenuation coefficient (*LAC*), half value layer (*HVL*), tenth value layer (*TVL*), effective atomic number (Z_{eff}), mean free path (*MFP*) using Phy-X/PSD software.
3. To study fast neutrons removable cross section (*FNRCS*) of clay bricks.
4. To study photon trajectory and gamma dose distribution using Particle and Heavy Ion Transport code System (PHITS).

Chapter 3

Materials and Methods

3.1 Sample collection

Sample of bricks are collected to investigate the radiation shielding properties of construction sites in the Kathmandu valley. For this purpose, five brick brand samples from different industries are collected from the construction site which are located in Pepsicola (Bhaktapur), Baneshwor (Kathmandu) and TU library (Kirtipur) are listed in Table 3.1.

Table 3.1: Co-ordinates of five different region from where samples were taken.

S.N.	Location	Brick Name	Latitude (degree)	Longitude (degree)
1	Kirtipur	Newa	27.669717	85.281633
2	Nayabajar	Harati	27.675285	85.281102
3	Baneshwor	Hira	27.688266	85.335061
4	Pepsicola	KTM	27.68819	85.361991
5	TU library	PK	27.681515	85.284437

Samples preparation

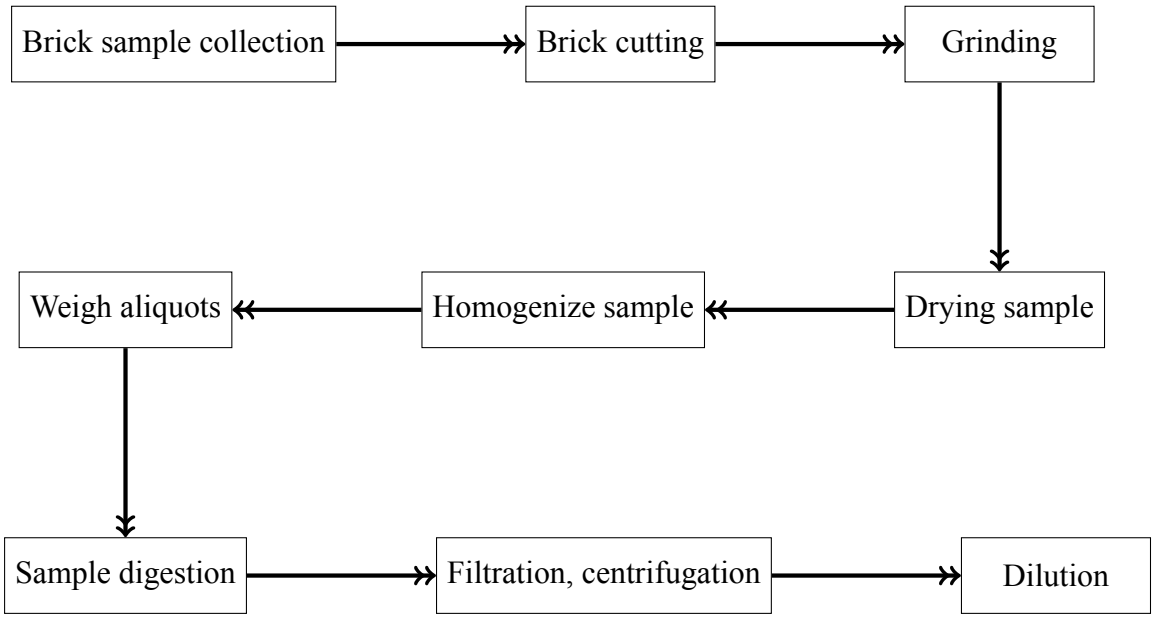

Samples were collected from various sites in Kathmandu and appropriately labeled. Slices of the sample were made with cutting machines. To prevent contamination, make sure the cutting equipment is clean. Wearing of protective clothing, such as gloves and goggles before start work. Mechanical grinder was used to crush. The brick was fragments into a fine powder and transfer them to the tiny container for chemical analysis. Drying sample helped to lose moisture. It was drying for 24 hours at 105 °C, or until the weight remains constant. Weigh the aliquots for exact and accurate sample quantities for digestion. Dissolve the brick powder into a solution for elemental analysis. Weighted sample in a digesting jar were added in mixture of concentrated acids (such as hydrochloric acid, hydrofluoric acid and nitric acid) then dissolve the brick matrix, heat the vessel in a microwave digestion system. Finally used a filter paper to filter the digested sample.

By modifying the concentration then dilution is ready for analysis. Place the centrifuged and filtered mixture in a volumetric flask. Dilute the solution by using deionized water or a diluent that is particular to the analytical technique to a known final volume. Well combine before removing aliquots for the last examination. Sample before and after preparation with their powder and dilution form are shown in Table 3.2.

Table 3.2: Samples before and after preparation with their powder and dilution form.

Sample name	Before preparation	After preparation	Powder form	Dilution
Newa				
Hariti				
Hira				
KTM				
PK				

ICP-OES

Full form of (ICP-OES) is Inductively Coupled Plasma-Optical Emission Spectrometry. It is widely used analytical techniques in the world. It determine trace and ultra trace elemental concentrations in the samples for multi-element analysis. It is applied in environmental monitoring, food analysis, microplastics, materials, human tissue, dietary supplements, body fluids and medical diagnostics. The majority of sample in ICP-OES are designed for liquid solutions. The procedures involved in the preparation of solid samples for ICP-OES analysis shows in Figure 3.1 ICP-OES used in the following ways: First, the quartz tube sparks when the argon gas passes through. It releases positively charged argon ions into the atmosphere. The radio frequency coil produces an oscillating magnetic field. Argon ions accelerate as a result. More argon ions are created when the argon ions collide with additional argon atoms. The resulting ionized gas is referred to as plasma.

When sample molecules or atoms are allowed to enter plasma, which has a temperature of roughly 6000 K, they release radiation, or emission spectra. This radiation is detected by a detector (wavelength). A computer analyzes the data before showing them. The components of ICP-OES are shown in Figure 3.1 b) [42].

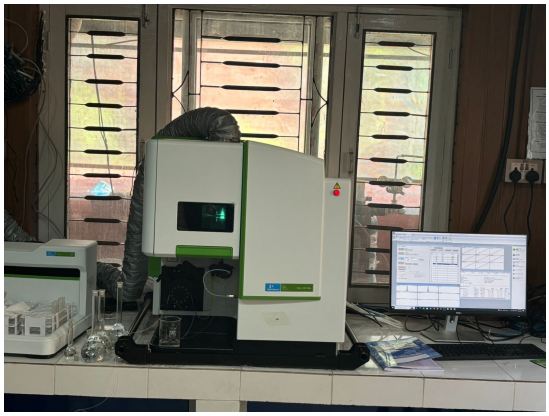

(a) ICP-OES instrument

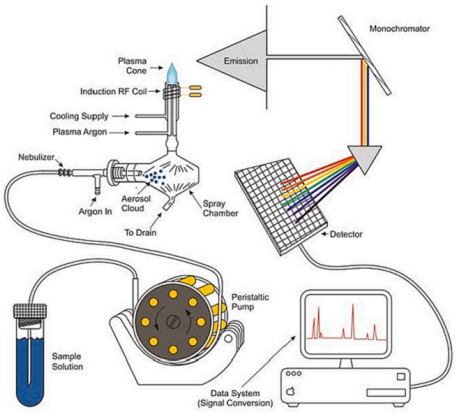

(b) Components of ICP-OES

Figure 3.1: Schematic diagram of ICP-OES.

Sample preparation includes grinding, dissolution, filtration and occasionally concentration techniques. The most popular method of dissolution of samples is acid digestion, which includes heating the sample in the presence of acid to promote metal solubilization [42].

3.2 Density of sample

Archimedes method

The bulk density of the brick was determined using the Archimedes principle. Three weights were measured on a single sample using the Archimedes method. w_{d} the dry sample weight, w_{sat} the fully saturated sample in a liquid (typically water) and w_{A} the saturated sample suspended and completely submerged in the weight of the saturating liquid (Archimedes weight). Figure 3.2 shows the density taking procedures followed in laboratory. The Archimedes weight (w_{A}) is used to derive the bulk density (ρ_b) as in Eq. (3.1) [43].

$$\rho_{\mathrm{b}} = \frac{w_{\mathrm{d}}\rho_{\mathrm{w}}}{w_{\mathrm{sat}} - w_{\mathrm{A}}} = \frac{m_{\mathrm{d}}}{V_{\mathrm{b}}} \tag{3.1}$$

here, ρ_{w} is the density of the liquid ρ_{b} bulk density of sample.

$$V_{\mathrm{b}} = \frac{(w_{\mathrm{sat}} - w_{\mathrm{A}})}{\rho_{\mathrm{w}}} \tag{3.2}$$

here, V_{b} bulk volume of sample.

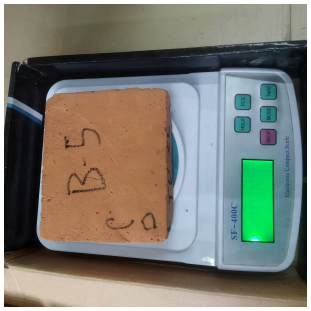

(a) Weight measurement of sample

(b) Saturating the sample

(c) Sample volume measurement

Figure 3.2: Steps for taking bulk density of sample.

3.3 Radiation shielding parameters

Linear Attenuation Coefficient (*LAC*)

When no brick specimens were placed between the source and the detector, the detector made its first measurement of gamma-ray intensity (N_0). The specimens were positioned between the source and the detector to measure the gamma-ray intensity (N) by the detector. An essential parameter that characterizes the penetration and diffusion of gamma radiation in a medium is the linear attenuation coefficient (μ) with unit cm^{-1}. The fraction of a gamma-radiation beam that is scattered or absorbed per unit thickness of the absorber is expressed by the linear attenuation coefficient (μ). The contributions from several physical processes (namely photoelectric effect, Compton scattering and pair creation) that might remove photons from the beam account for the total linear attenuation coefficient (μ) for photons of a given energy in a particular material. By normalizing the linear attenuation coefficient (μ) with respect to the absorber density (ρ), one may obtain its dependency on the absorber density [44]. The linear attenuation coefficient was measured using a formula.

$$\mu = \frac{1}{x} \ln \frac{N_0}{N} \tag{3.3}$$

where,

μ = linear attenuation coefficient

x= material thickness in cm

Mass attenuation coefficient (*MAC*)

The well-known Beer Lambert rule, found in Eq. (3.4), may be used to determine the mass attenuation coefficient (MAC) (μ_m), which expresses the interaction probability between photons

and the mass per unit area for a particular medium as in Eq. (3.5) [45].

$$I = I_0 e^{-\mu t} \tag{3.4}$$

$$\mu_m = \left(\frac{\mu}{\rho}\right) = \frac{ln(I_0/I)}{\rho t} \tag{3.5}$$

where I_0 and I are unattenuated and attenuated photon intensities, μ (cm^{-1}) and μ_m (cm^2 g^{-1}) are linear and mass attenuation coefficients, t (cm) and ρ (g cm^{-3}) are the thickness and density of material.

For mixture and compound, we use Eq. (3.6)

$$\mu_{\mathrm{m}} = \left(\frac{\mu}{\rho}\right) = \sum_i W_i \left(\frac{\mu}{\rho}\right)_i \tag{3.6}$$

where w_i and $(\mu/\rho)_i$ are the weight fraction and the mass attenuation coefficient of the constituent element i^{th}, respectively. The mass attenuation coefficient $\frac{\mu}{\rho}$ is really of more fundamental value than the linear coefficient, because it does not depend on the actual density and physical state of the absorber [4].

Mean free path

Mean free path (*MFP*) is another factor that affects radiation shielding properties and is defined as the average distance a particle (atom, molecule, photon) travels between successive collisions with other particles. *MFP* is calculated using the Eq. (3.7) [46].

$$MFP = \frac{1}{\mu} \tag{3.7}$$

where μ is linear attenuation coefficient.

Half Value Layer

The material's half value layer (*HVL*), or thickness per unit, plays a significant role in defining its shielding properties. The thickness that reduces 50% of the radiation that passes through the material is indicated by the symbol *HVL*. Using Eq. (3.8), the *HVL* value can be found [47].

$$HVL = \frac{0.693}{\mu} \tag{3.8}$$

Tenth value layer

The tenth value layer (*TVL*) defines the thickness of the material that decreases the radiation passing by a factor of one tenth of the initial value. The Eq. (4.11) is for determination of *TVL*.

$$TVL = \frac{2.302}{\mu} \tag{3.9}$$

Atomic cross section

Total atomic cross section (*ACS*) is the sum of all cross section by which electron interacts with the atom. ACS can be evaluated from given Eq. (3.10) [48].

$$ACS = \frac{(\mu/\rho)_{alloy}}{N_A \sum_i \frac{w_i}{A_i}} \tag{3.10}$$

where A_i, w_i is the atomic weight and weight fraction of each element in the mixture. N_A is Avogadro's Number.

Electronic cross section

Total electronic cross section (*ECS*) is the cross section by which electron interacts with the photon. Eq. (3.11) determines the *ECS* value.

$$ECS = \frac{1}{N_A} \sum_i \frac{F_i A_i}{Z_i} (\frac{\mu}{\rho})_i \tag{3.11}$$

where Z_i, F_i, $(\mu/\rho)_i$ and A_i are the atomic number, mole fraction, mass attenuation coefficient and atomic weight of the i^{th} constituent element, respectively.

Effective atomic number

Another number to consider for a material made of various elements is the effective atomic number (*EAN*) (Z_{eff}), which applies to glasses. The formula for computing it is Eq. (3.12) [49].

$$Z_{\text{eff}} = \frac{\sum_i F_i A_i (\mu/\rho)_i}{\sum_j F_j (A_j/Z_j)(\mu/\rho)_j} = \frac{ACS}{ECS} \tag{3.12}$$

Effective Electron Density

To compute the effective electron density (N_{eff}), utilize Eq. (3.13) [50].

$$N_{\text{eff}} = \frac{\mu_m}{ECS} \tag{3.13}$$

where μ_m is the mass attenuation coefficient and *ECS* is electronic cross section.

Effective Conductivity

Effective conductivity (C_{eff}) of the glass material is related to the effective electron density (N_{eff}) through Eq. (3.14) [50].

$$C_{\text{eff}} = \left(\frac{N_{\text{eff}}\rho\tau e^2}{m_e}\right)10^3 \tag{3.14}$$

where e (C) and m_e (kg) are charge and mass of electron respectively and τ is the average life time of the electron on the Fermi surface.

3.4 Theoretical method

Phy-X/PSD

For the calculation of different radiation attenuation parameters, we uses Phy-X / PSD software in the energy range 15 keV to 15 MeV [51]. The data obtained are plotted in graph using Python programming. Representative of photon shielding and dosimetry software Phy-X/PSD is shown in Figure 3.3.

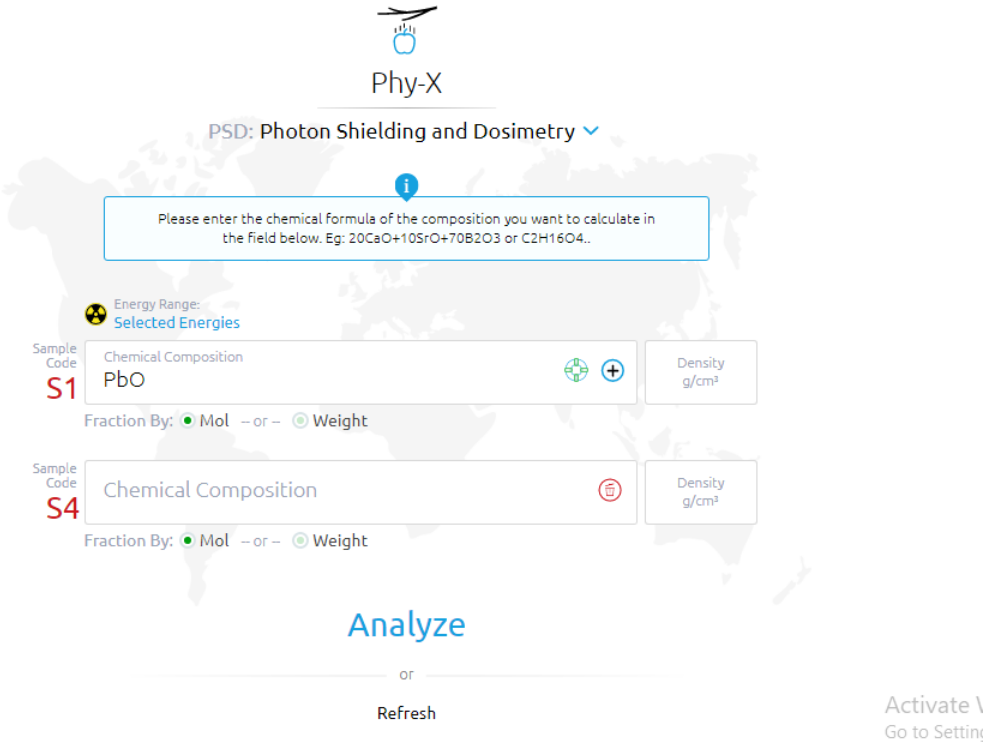

Figure 3.3: Phy-X/PSD online software.

Particle and Heavy Ion Transport Code System (PHITS)

We use PHITS (Particle and Heavy Ion Transport Code System) software for simulation. The representation of PHITS is shown in Figure 3.4 [52].

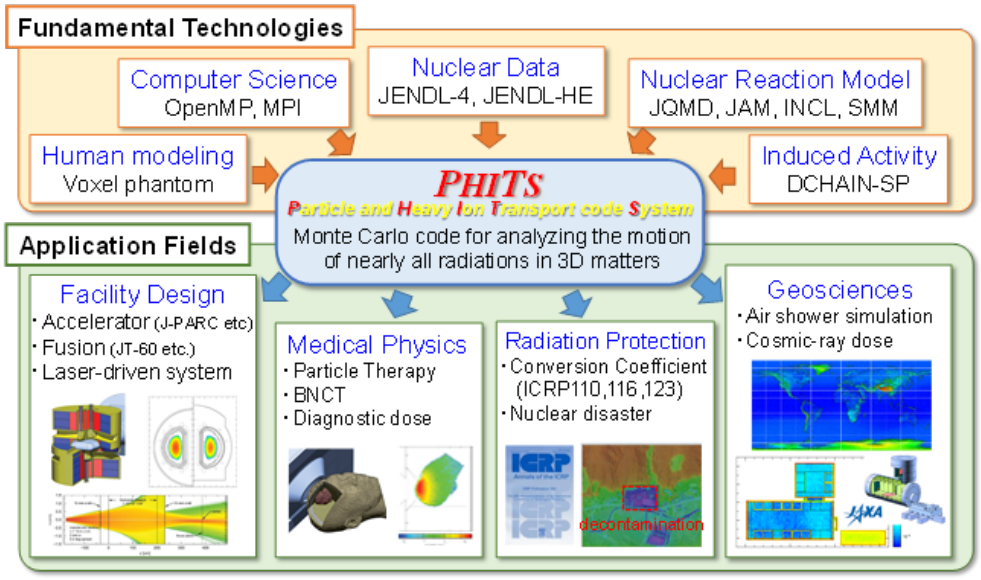

Figure 3.4: Particle and heavy ion transport code system.

Particle and heavy-ion transport code system transport and collision of nearly all particles (neutron, proton, ions, electrons and photons) over wide energy range (10^{-4} eV to 1 TeV) using Monte Carlo method. The Monte Carlo method trace the motion of each particle using a random number and estimate its average behavior by iterating the simulation. Monte Carlo simulation is a mathematical approach that is used to model risk or uncertainty in a given system by creating random variables. Based on probability distributions such as normal and log normal, among others, random variables or inputs are simulated [53].

3.5 Data analysis

The data from gamma-spectrometer was analyzed and compiled using Python computer programming. Python, developed by Guido van Rossum in 1991, is a popular high-level interpreted language suitable for web development, data science, automation and more due to its ease of learning and wide range of applications.

Chapter 4

Results and Discussion

4.1 Chemical composition and density of bricks

Density and chemical composition of the brick samples are listed in Table 4.1. The chemical composition of the brick samples listed in the table is recognized using ICP-OES and the bulk density is measured in a laboratory using Archimedes's principle as described in methodology section 3.2.

Table 4.1: Element concentration and density of brick samples.

Element	**Newa**	**Harati**	**Hira**	**KTM**	**PK**
Density (g cm^{-3})	1.49	1.71	1.74	1.54	1.57
	Weight percent (wt%)				
Al	0.71	4.77	2.07	2.75	1.58
Si	55.29	58.92	68.13	64.97	38.25
P	0.02	0.14	0.17	0.17	0.06
Ca	1.07	0.18	0.22	0.23	0.23
Mg	0.18	0.07	0.04	0.04	0.06
Na	0.16	0.16	2.09	0.54	0.13
K	0.17	2.06	2.21	1.69	0.75
Fe	0.83	4.47	2.76	2.98	1.67
Mn	0.01	0.05	0.03	0.03	0.02
Ti	0.05	0.49	0.37	0.41	0.21

4.2 Radiation shielding parameters

After analyzing the chemical composition of the brick samples by ICP-OES, we used the Phy-X/PSD software with an energy range of 15 keV to 15 MeV for calculating radiation shielding characteristics. Based on the data acquired, a variety of graphs are produced. A review of the collected data and graph are provided below. The mass attenuation coefficients (*MAC*) of five selected samples, known as Newa, Harati, Hira, KTM and PK were calculated and presented on a graph, as shown in Figure 4.1 a). Similarly, the linear attenuation coefficient of five selected brick samples is obtained and plotted on a graph as shown in Figure 4.1 b).

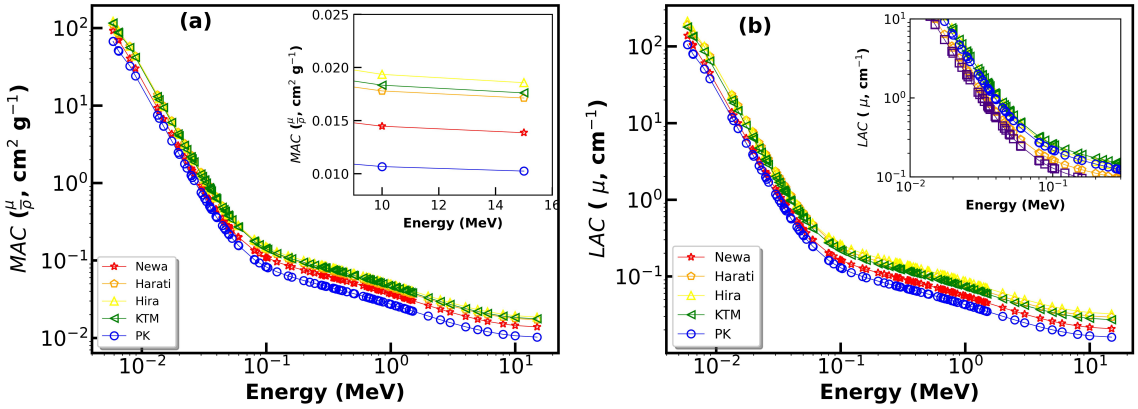

Figure 4.1: (a) *MAC* of five brick samples versus photon energy. (b) *LAC* of five brick samples versus photon energy.

At maximum energy 15 MeV value of *MAC* obtained for the brick samples Newa, Harati, Hira, KTM and PK are 0.93×10^{2} cm^{2} g^{-1}, 1.12×10^{2} cm^{2} g^{-1}, 1.23×10^{2} cm^{2} g^{-1}, 1.16×10^{2} cm^{2} g^{-1} and 0.67×10^{2} cm^{2} g^{-1} respectively. Also at minimum energy 0.58×10^{-2} MeV value of *MAC* obtained are 1.38×10^{-2} cm^{2} g^{-1}, 1.71×10^{-2} cm^{2} g^{-1}, 1.86×10^{-2} cm^{2} g^{-1}, 1.76×10^{-2} cm^{2} g^{-1} and 1.24×10^{-2} cm^{2} g^{-1} for respective five samples. The average energy 8.63×10^{2} keV value of *MAC* obtained are 0.46×10^{1} cm^{2} g^{-1}, 0.58×10^{1} cm^{2} g^{-1}, 0.62×10^{1} cm^{2} g^{-1}, 0.59×10^{1} cm^{2} g^{-1} and 0.34×10^{1} cm^{2} g^{-1} for respective five samples.

The results of five samples show that PK has the lowest value of *MAC* while Hira brand brick has a high value of *MAC*. This suggests that the Hira brand brick has high radiation shielding capacity and the PK brand brick has low radiation shielding capacity.

The maximum value of *LAC* obtained for the sample Newa, Harati, Hira, KTM and PK at energy 15 MeV are 1.38×10^{2} cm^{-1}, 1.91×10^{2} cm^{-1}, 2.13×10^{2} cm^{-1}, 1.79×10^{2} cm^{-1} and 1.06×10^{2}

cm^{-1} respectively. At minimum energy 0.59×10^{-2} MeV, *LAC* value are 2.06×10^{-2} cm^{-1}, 2.92×10^{-2} cm^{-1}, 3.23×10^{-2} cm^{-1}, 2.71×10^{-2} cm^{-1} and 1.60×10^{-2} cm^{-1} for respective five samples. Also at mean energy 0.86 MeV, *LAC* value are 0.68×10^{-1} cm^{-1}, 0.99×10^{-1} cm^{-1}, 1.08×10^{-1} cm^{-1}, 0.91×10^{-1} cm^{-1} and 0.54×10^{-1} cm^{-1} for respective five samples.

According to the value obtained from our five samples, Hira has the highest *LAC* value and PK has the lowest *LAC* value.

The measured value and graph show that for low energy range the sample gives the best shielding. Low value of *LAC* shows that best shielding of sample. The *LAC* value decreases for the simple brick as the energy increases. We acquired maximum *LAC* values at low energy and minimum *LAC* values at high energy (15 MeV) for five samples, as we know that *LAC* values are based on the density of brick samples and *MAC* values.

Half Value Layer

An important parameter for the study of penetration of photon radiation is the half-value layer (*HVL*). The *HVL* graph is plotted and shown in Figure 4.2. The graph shows that the half-value layer increases linearly with energy. In addition many other previous work indicates that for better shielding capacity the *HVL* should be as small as possible.

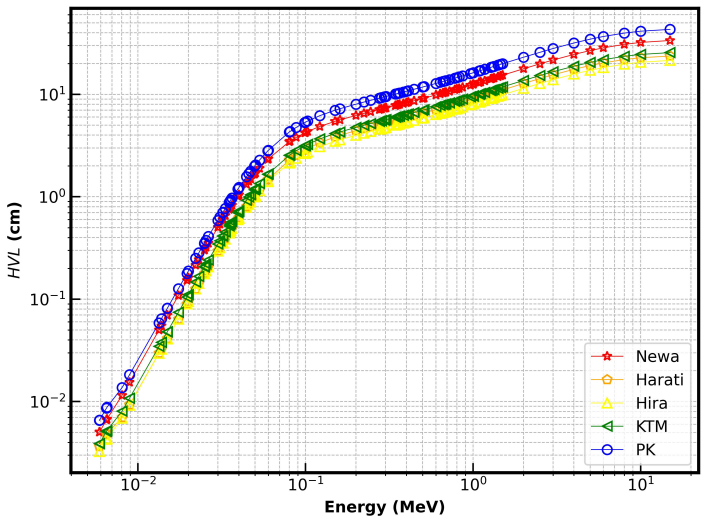

Figure 4.2: Photon energy versus *HVL* of the five brick sample.

For selected samples the at maximum energy 15 MeV value of *HVL* obtained for the sample Newa, Harati, Hira, KTM and PK are 0.33×10^{2} cm, 0.24×10^{2} cm, 0.210×10^{2} cm, 0.25×10^{2}

cm and 0.43×10^{2} cm respectively. At minimum energy 0.58×10^{-2} MeV, *HVL* value are 0.50×10^{-2} cm, 0.36×10^{-2} cm, 0.33×10^{-2} cm, 0.39×10^{-2} cm and 0.66×10^{-2} cm for respective five samples. At average energy 8.63×10^{2} keV, *HVL* value are 0.73×10^{-1} cm, 0.52×10^{-1} cm, 0.46×10^{-1} cm, 0.55×10^{-1} cm and 0.94×10^{-1} cm for respective five samples.

Thus, from obtained data, we can conclude that Hira brand brick has lowest *HVL* and PK brand brick has the highest *HVL* value, which suggests that sample Hira contains the best shielding properties among our five sample and PK contains the least photon shielding properties.

Tenth value layer

Another important parameter is for study of penetration of photon radiation is the tenth value layer (*TVL*). The graph for *TVL* is plotted and shown in Figure 4.3. The graph depicts that the tenth value layer increases linearly with energy. Also many other previous work indicates that for better shielding capacity, the *TVL* value should be as small as possible.

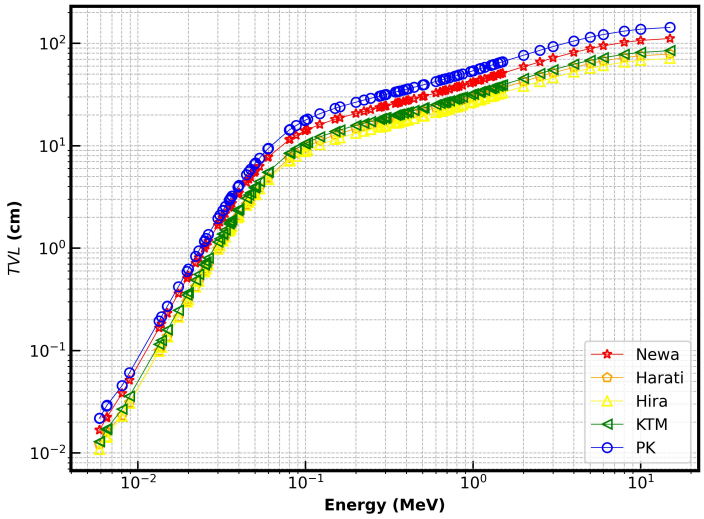

Figure 4.3: Photon energy versus tenth value layer (*TVL*) of five brick sample.

For selected samples at maximum energy 15 MeV, *TVL* value obtained for the sample Newa, Harati, Hira, KTM and PK are 1.11×10^{2} cm, 0.79×10^{2} cm, 0.71×10^{2} cm, 0.85×10^{2} cm and 1.43×10^{2} cm respectively, also at minimum energy 0.59×10^{1} keV, *TVL* values are 1.67×10^{-2} cm, 1.21×10^{-2} cm, 1.08×10^{-2} cm, 1.29×10^{-2} cm and 2.18×10^{-2} cm for respective five samples. Also, at average energy 8.62×10^{2} keV, *TVL* values are 0.24×10^{2} cm, 0.17×10^{2} cm, 0.15×10^{2} cm, 0.18×10^{2} cm and 0.31×10^{2} cm for respective five samples.

Thus, from the data obtained we can conclude that Hira brand brick has the lowest *TVL* and

PK has the highest *TVL* value, which suggest that sample Hira contain best shielding properties among our five sample and PK contain least photon shielding properties.

Mean free path

Mean free path (*MFP*) is another relevant parameter in determining photon attenuation properties. The obtained data from Phy-X/PSD is plotted in graph as shown in Figure 4.4. The graph depicts that the *MFP* increases linearly with energy. Also many other previous work indicates that for better shielding capacity the *MFP* should be as small as possible [54].

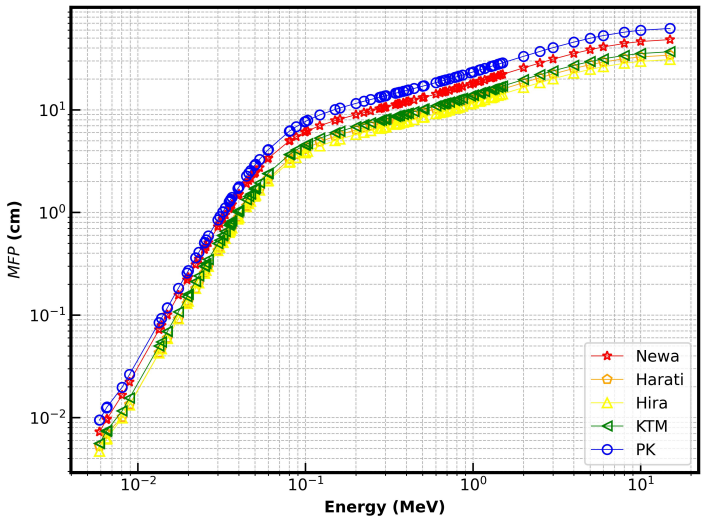

Figure 4.4: Photon energy versus mean free path (*MFP*) of the five brick sample.

For selected samples the maximum energy 15 MeV value of *MFP* obtained for the sample Newa, Harati, Hira, KTM and PK are 48.42 cm, 34.14 cm, 30.95 cm, 36.88 cm and 62.17 cm respectively and at the minimum energy 0.58×10^{1} keV *MFP* value are 0.72×10^{-2} cm, 0.52×10^{-2} cm, 0.47×10^{-2} cm, 0.56×10^{-2} cm and 0.95×10^{-2} cm for respective five samples. At average energy 8.63×10^{2} keV *MFP* value are 10.49 cm, 7.45 cm, 6.72 cm, 8.02 cm and 13.15 cm for respective five samples.

Thus, from obtained data we can conclude that PK brick brand has highest MPF and Hira brick brand has lowest MFP value, suggesting that Hira contains the best shielding properties among five samples and PK brick brand has least gamma ray shielding properties. *MFP* value is significantly affected by density value so that *MFP* reduces with increasing the density. *MFP* has inverse relation with LAC [55].

Effective atomic number

For selected samples at maximum energy 15 MeV value of effective atomic number (Z_{eff}) obtained for the sample Newa, Harati, Hira, KTM and PK are 14.75, 16.36, 15.50, 15.65 and 15.59 respectively also at low energy 5.8 keV effective atomic number value are 14.15, 14.47, 14.23, 14.31 and 14.30 for respective five samples. At average energy 862.6 keV effective atomic number values are 14.37, 15.15, 14.69, 14.79 and 14.76 for respective five samples. Figure 4.5 shows Z_{eff} against different value of photon energy.

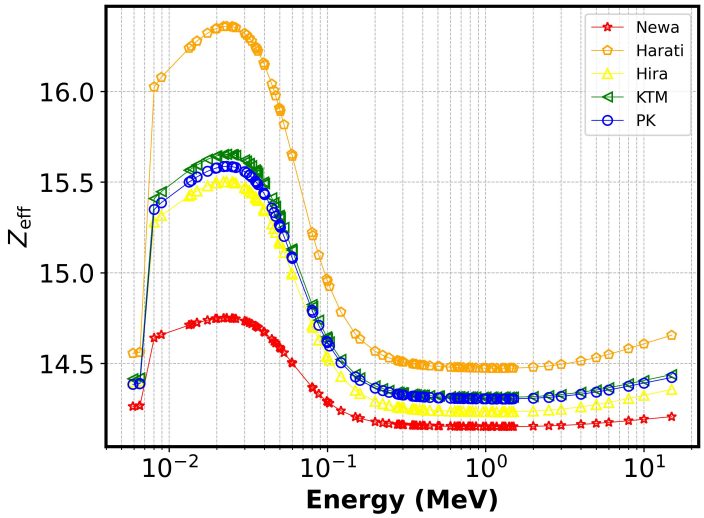

Figure 4.5: Z_{eff} versus photon energy.

We obtained maximum Z_{eff} for Harati have highest value which is maximum and Newa sample has minimum value. Therefore, from data, we can conclude that Harati has high Z_{eff} value Newa contains the least Z_{eff} value.

Effective electron density

The graphical representation of the effective electron density against different values of photon energy is shown in Figure 4.6.

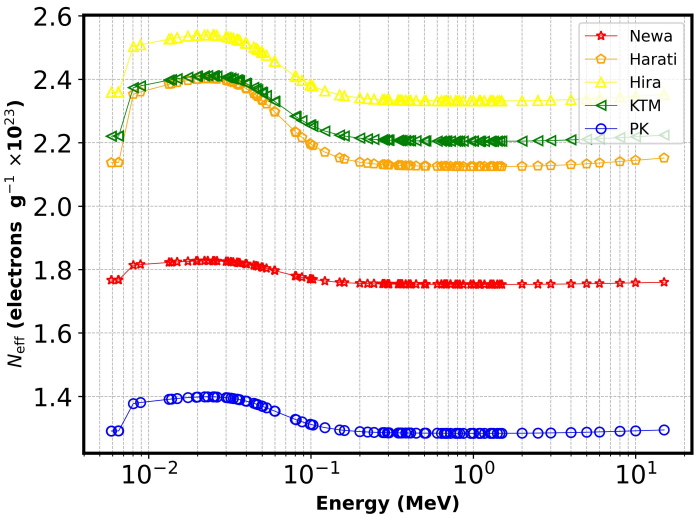

Figure 4.6: N_{eff} versus photon energy.

For selected samples the at maximum energy 15 MeV value of effective electron density (N_{eff}) obtained for the sample Newa, Harati, Hira, KTM and PK are 1.83×10^{23} electrons g^{-1}, 2.40×10^{23} electrons g^{-1}, 2.53×10^{23} electrons g^{-1}, 2.41×10^{23} electrons g^{-1} and 1.39×10^{23} electrons g^{-1} respectively and at minimum energy 5.8 keV, N_{eff} value are 1.75×10^{23} electrons g^{-1}, 2.12×10^{24} electrons g^{-1}, 2.33×10^{23} electrons g^{-1}, 2.20×10^{23} electrons g^{-1}, 1.28×10^{23} electrons g^{-1} . Also at average energy 8.63×10^{2} keV, N_{eff} value are 1.77×10^{23} electrons g^{-1}, 2.22×10^{22} electrons g^{-1}, 2.40×10^{23} electrons g^{-1}, 2.27×10^{23} electrons g^{-1}, 1.32×10^{23} electrons g^{-1} . We have obtained maximum N_{eff} for Hira have highest value which is maximum and PK sample has minimum value. Therefore, from our data we can conclude that Hira has high N_{eff} value PK contain least N_{eff} value.

Effective conductivity

The graphical representation for effective conductivity (C_{eff}) against different value of photon energy is shown in Figure 4.7.

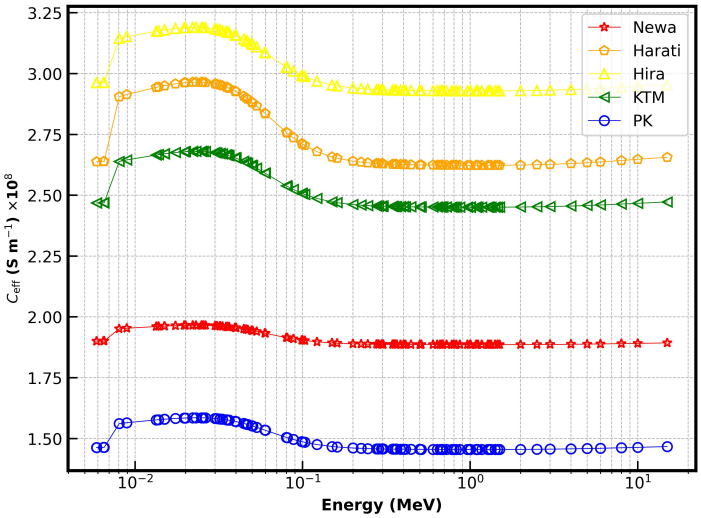

Figure 4.7: Effective conductivity (C_{eff}) versus photon energy.

At maximum energy 15 MeV value of Effective Conductivity (C_{eff}) for the sample Newa, Harati, Hira, KTM and PK are 1.96×10^{8} S m^{-1}, 2.96×10^{8} S m^{-1}, 3.19×10^{8} S m^{-1}, 2.68×10^{8} S m^{-1}, 1.58×10^{8} S m^{-1} respectively and at minimum energy 5.80 keV value of effective conductivity (C_{eff}) are 1.88×10^{8} S m^{-1}, 2.62×10^{8} S m^{-1}, 2.92×10^{8} S m^{-1}, 2.45×10^{8} S m^{-1}, 1.45×10^{8} S m^{-1} for respective five samples. At energy 8.63×10^{2} keV value of effective conductivity (C_{eff})) are 1.91×10^{8} S m^{-1}, 2.74×10^{8} S m^{-1}, 3.02×10^{8} S m^{-1}, 2.53×10^{8} S m^{-1}, 1.50×10^{8} S m^{-1} for respective five samples.

N_{eff} and C_{eff} both contain highest value at low energy and later decreases upto 15 keV and increases slowly upto 15 MeV. A similar pattern of the graph are obtained as Z_{eff}.

Fast neutron removal cross-Section

The graphical representation for Fast Neutron Removal Cross-Section is shown in Figure 4.8. The (*FNRCS*) measures the potential for a fast neutron to be extracted from a beam during its passage through a material. Fission, absorption, or scattering inside the nucleus of the material are a few of the interactions that might lead to this elimination. The atomic structure of a material and the neutron energy affect the removal cross section [56]. The fast neutron removal cross section values for different brand brick samples are shown in Table 4.2.

Table 4.2: Fast neutron removal cross-section

Sample	Newa	Harati	Hira	KTM	PK
FNRCS (cm^{-1})	2.55×10^{-2}	3.51×10^{-2}	3.96×10^{-2}	3.30×10^{-2}	1.96×10^{-2}

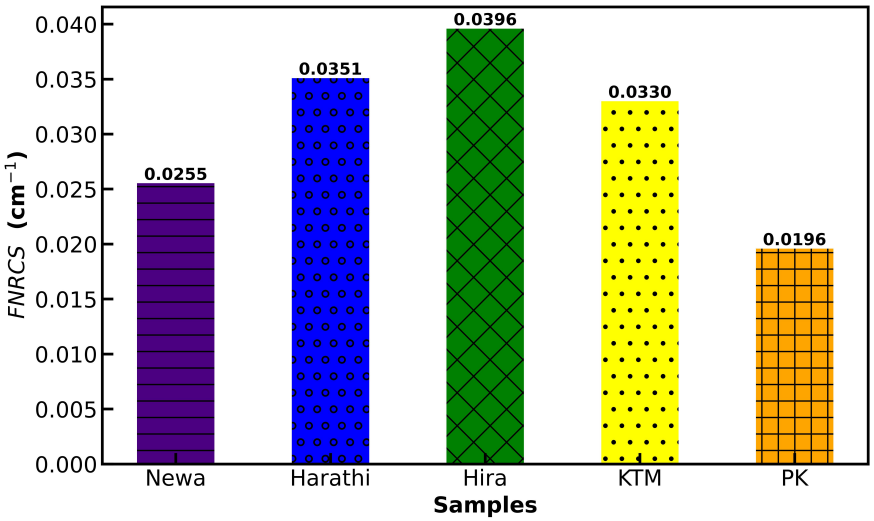

Figure 4.8: Brick samples and its fast neutron removal cross section.

From the graph we reach in conclusion that among the five bricks sample Hira has highest value of *FNRCS* and PK has low value of *FNRCS*. After analysis the data we can reach in a conclusion that Hira brick has best radiation shielding capacity and PK has last radiation shielding capacity.

4.3 Linear attenuation coefficient of bricks associated with gamma energy from radionuclides

Table 4.3 shows linear attenuation coefficient of bricks associated with gamma energy from radionuclides. The *LAC* values of the five selected samples are shown in Figure 4.9. All of these values correspond to the energy peak of common radionuclei, such as Americium (^{241}Am), Europium (^{152}Eu), Cesium (^{137}Cs) and Cobalt (^{60}Co), that are useful for a variety of applications in medical facilities, industrial radiography and research institutes. Tests of the material's shielding ability reveal that photoelectric effects predominate up to (^{241}Am) source photon. Figure 4.9 displays the data that has been analyzed.

Table 4.3: Illustration of the linear attenuation coefficient of bricks against gamma energy from radioactive nuclei ^{154}Eu, ^{137}Cs, ^{241}Am and ^{60}Co.

Energy (MeV)	Nuclide Symbol	*LAC* (cm^{-1})				
		Newa	**Harati**	**Hira**	**KTM**	**PK**
1.38×10^{-2}	^{241}Am	12.61	21.31	21.37	18.27	10.75
2.36×10^{-2}	^{241}Am	1.97	3.37	3.36	2.87	1.69
4.59×10^{-2}	^{152}Eu	0.49	0.81	0.82	0.70	0.41
1.22×10^{-1}	^{152}Eu	0.14	0.20	0.22	0.19	0.11
2.84×10^{-1}	^{137}Cs	0.10	0.13	0.15	0.13	0.07
3.44×10^{-1}	^{152}Eu	0.09	0.12	0.14	0.12	0.07
6.62×10^{-1}	^{137}Cs	0.07	0.09	0.10	0.09	0.05
8.26×10^{-1}	^{60}Co	0.06	0.08	0.09	0.08	0.05
1.17	^{60}Co	0.05	0.07	0.08	0.07	0.04
1.33	^{60}Co	0.05	0.07	0.07	0.06	0.04
2.51	^{60}Co	0.03	0.05	0.05	0.05	0.03

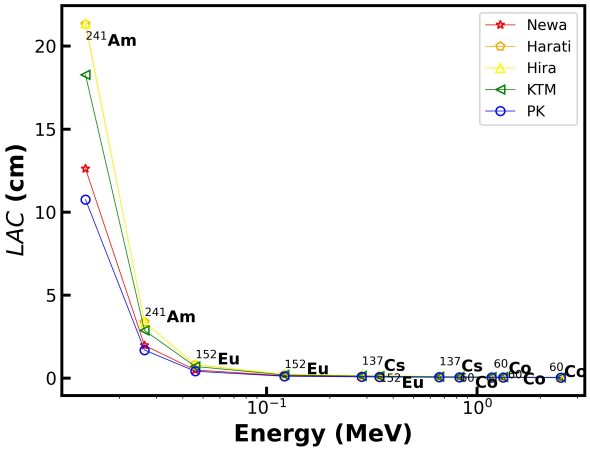

Figure 4.9: Linear attenuation coefficients versus gamma ray photons from technically enhanced radionuclides (^{241}Am, ^{152}Eu, ^{137}Cs and ^{60}Co).

4.4 Mean free path of bricks associated with gamma energy from radionuclei

The mean free path (MFP) values of the five selected samples are shown in Figure 4.10. All of these values correspond to the energy peak of common radionuclei, such as Americium (^{241}Am), Europium (^{152}Eu), Cesium (^{137}Cs) and Cobalt (^{60}Co), that are helpful for a variety of reasons in medical facilities, industrial radiography and several research facilities. When the shielding properties of the material are examined, photoelectric effects become dominant up to ^{241}Am source photon Figure 4.10 displays the data analysis. Table 4.4 shows the mean free path and related gamma energy from radioactive nuclei.

Table 4.4: Illustration of the mean free path and related gamma energy from radioactive nuclei ^{154}Eu, ^{137}Cs, ^{241}Am and ^{60}Co.

Energy (MeV)	Nuclide Symbol	*MFP* (cm)				
		Newa	**Harati**	**Hira**	**KTM**	**PK**
1.38×10^{-2}	^{241}Am	0.08	0.05	0.05	0.05	0.09
2.36×10^{-2}	^{241}Am	0.51	0.29	0.29	0.34	0.59
4.59×10^{-2}	^{152}Eu	2.04	1.24	1.22	1.43	2.43
1.22×10^{-1}	^{152}Eu	7.01	4.87	4.45	5.29	8.93
2.84×10^{-1}	^{137}Cs	10.36	7.42	6.66	7.95	13.40
3.44×10^{-1}	^{152}Eu	11.22	8.04	7.22	8.62	14.52
6.62×10^{-1}	^{137}Cs	14.86	10.68	9.57	11.43	19.26
8.26×10^{-1}	^{60}Co	16.47	11.84	10.60	12.67	21.35
1.17	^{60}Co	19.56	14.06	12.59	15.05	25.35
1.33	^{60}Co	20.87	15.00	13.44	16.06	27.05
2.51	^{60}Co	28.65	20.56	18.43	22.02	37.10

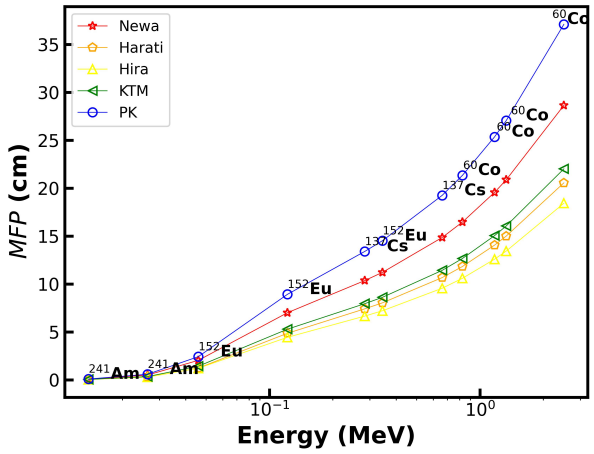

Figure 4.10: Mean free path of the gamma-ray photons inside the brick sample versus technically enhanced radionuclei such as ^{241}Am, ^{152}Eu, ^{137}Cs and ^{60}Co.

4.5 Tenth value layer of bricks associated with gamma energy from radionuclei.

All of these values correspond to the energy peak of common radionuclei, such as Americium (^{241}Am), Europium (^{152}Eu), Cesium (^{137}Cs) and Cobalt (^{60}Co), that are beneficial for many

uses in research institutions, industrial radiography and medical facilities. When the shielding properties of the material are examined, photoelectric effects become dominant up to source photon Figure 4.11 displays the data analysis. Table 4.5 shows that tenth value layer associated with gamma energy from radionuclide.

Table 4.5: Representation of the tenth value layer associated with gamma energy from radionuclei ^{241}Am, ^{152}Eu, ^{137}Cs and ^{60}Co.

Energy (MeV)	Nuclide Symbol	*TVL* (cm)				
		Newa	**Harati**	**Hira**	**KTM**	**PK**
1.38×10^{-2}	^{241}Am	0.18	0.11	0.11	0.13	0.21
2.36×10^{-2}	^{241}Am	1.17	0.68	0.69	0.80	1.36
4.59×10^{-2}	^{152}Eu	4.70	2.85	2.81	3.29	5.59
1.22×10^{-1}	^{152}Eu	16.15	11.21	10.24	12.19	20.57
2.84×10^{-1}	^{137}Cs	23.86	17.07	15.33	18.31	30.86
3.44×10^{-1}	^{152}Eu	25.84	18.52	16.62	19.85	33.44
6.62×10^{-1}	^{137}Cs	34.22	24.58	22.03	26.32	44.34
8.26×10^{-1}	^{60}Co	37.93	27.26	24.42	29.18	49.15
1.17	^{60}Co	45.04	32.37	28.99	34.65	58.37
1.33	^{60}Co	48.07	34.55	30.95	36.98	62.29
2.51	^{60}Co	65.96	47.34	42.44	50.71	85.43

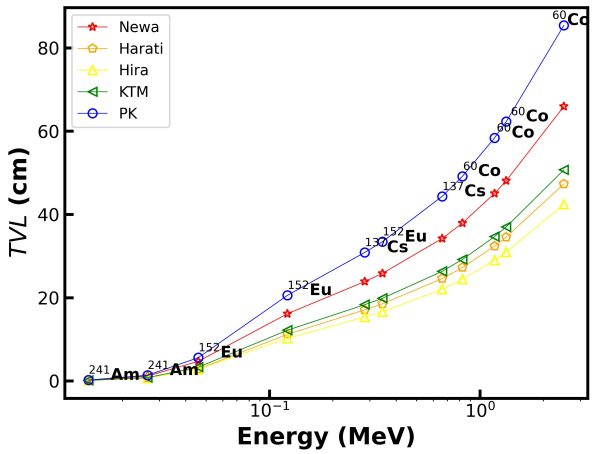

Figure 4.11: Tenth value layer of gamma ray photons versus technically enhanced radionuclei such as ^{241}Am, ^{152}Eu, ^{137}Cs and ^{60}Co.

4.6 Comparison with past work

Table 4.6 shows comparison between simulated PhyX/PSD work at energy 0.66 MeV of ^{137}Cs and 1.17, 1.33 MeV of ^{60}Co with past work done by Thuong et al.(2024). Theoretical works and experimental work are comparable.

Table 4.6: Comparative study of linear attenuation coefficient of bricks brand and reference brick

	LAC (cm^{-1})					
Energy (MeV)	Newa	Harati	Hira	KTM	PK	Reference [31]
0.66	0.07	0.09	0.10	0.08	0.05	0.11
1.17	0.05	0.07	0.08	0.07	0.04	0.08
1.33	0.05	0.05	0.07	0.06	0.04	0.07
Density (g cm^{-3})	1.49	1.71	1.74	1.54	1.57	1.98

4.7 Photon trajectory in brick sample.

In Figure 4.12 a) represent the maze geometry of the system which consists inner region air of (20% O_2 and 80% N_2) and outer region of Hira brick. Figure b) one million photon bombardment at 1 ns originated from 200 GBq activity from ^{137}Cs. Figure c) represent the dose distribution inside maze at the dose at 27 ns. Figure d) shows the dose distribution inside the maze at 42 ns from (^{137}Cs). Using PHITS Monte Carlo method in Figure 4.12 shows the 1 million photon trajectories in the sample of Hira bricks after 1 ns, 21 ns and 48 ns.

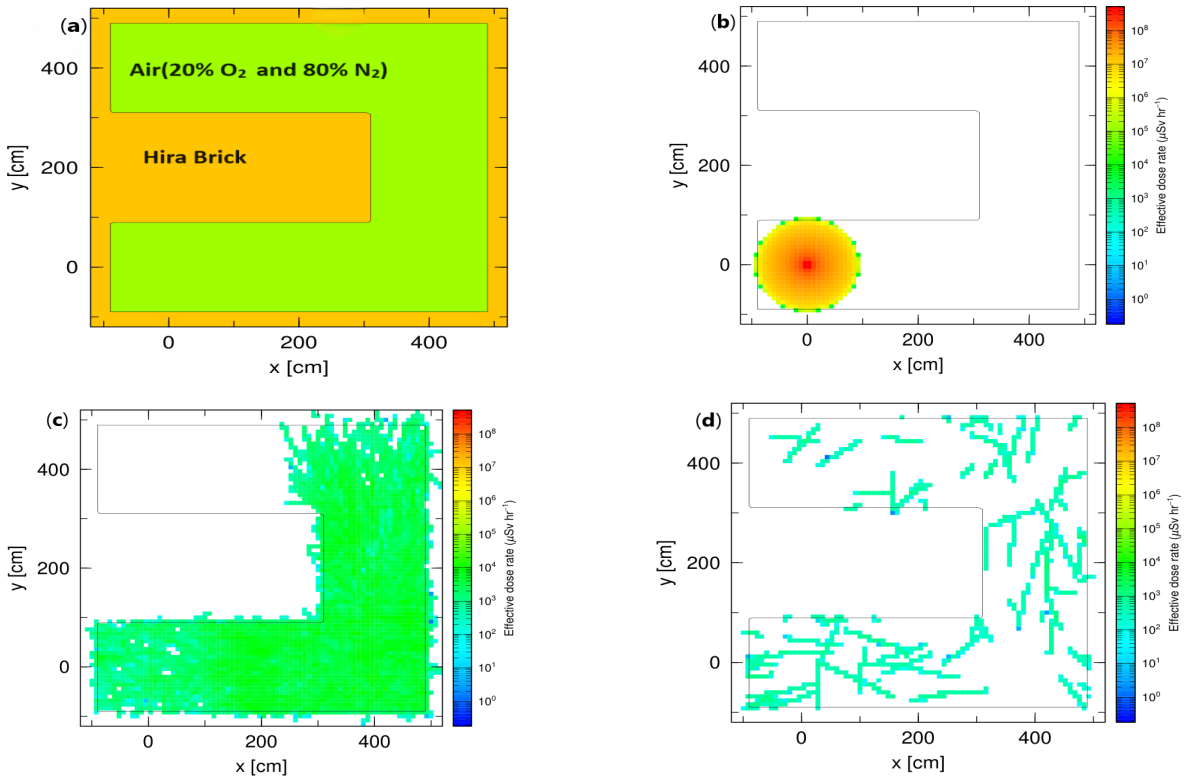

Figure 4.12: Photon trajectory and dose distribution inside the Hira brick sample.

Chapter 5

Conclusion

Physical properties such as density of five clay brick brands named Newa, Harati, Hira, KTM and PK have been studied and chemical properties have been studied using inductively coupled plasma optical emission spectroscopy (ICP-OES). The radiation shielding parameters of selected brick brand named Newa, Harati, Hira, KTM and PK have been studied using online based Phy-X/PSD software in an energy range of 15 keV to 15 MeV. Also the *MAC* value and *LAC* value obtained by Phy-X / PSD are plotted on the graph and found a similar pattern on the graph of the *MAC* and *LAC*. Both *MAC* and *LAC* values are found to be maximum in the low energy 15 keV and minimum in the high energy 15 MeV. From the result we obtained that low the value for *HVL*, *TVL*, *MFP* has the high shielding properties. Among five samples Hira has high mass attenuation value and minimum *HVL*, *TVL* and *MFP* value is obtained. The linear relationship between N_{eff} and C_{eff} with Z_{eff} is observed. By analyzing all data and graph we conclude that sample Hira is the best shielding brick among five samples and PK has the least radiation shielding ability. Among the five clay bricks the fast neutron shielding cross section of Hira brand brick is highest which is 3.96×10^{-2} cm^{-1} and lowest is in KTM brand brick which is 1.96×10^{-2} cm^{-1}.

5.1 Future work

In future our work can be further studied in the following ways:

- Fabrication of radiation shielding systems with better performance characteristics may be developed by dopping different clay minerals in Bricks.

- Understanding how the distinctive features of clay materials contribute to their efficiency as radiation shields may be gained by conducting a nanoscale analysis of their structural properties.
- Investigating the interplay between clay minerals and other additives, like polymers or nanoparticles, may present novel approaches to enhancing the overall robustness and adaptability of radiation-shielding materials in a range of environmental scenarios.

References

[1] E. J. Hall, A. J. Giaccia, *et al.*, *Radiobiology for the Radiologist*, Vol. 6 (Philadelphia, 2006).

[2] M. M. Al-Bared and A. Marto, Mal. J. Fund. Appl. Sci. **13**, 825 (2017).

[3] N. Ural, *The importance of clay in Geotechnical Engineering* (IntechOpen London, UK:, 2018).

[4] S. Olukotun, S. Gbenu, F. Ibitoye, O. Oladejo, H. Shittu, M. Fasasi, and F. Balogun, Nucl. Eng. Technol. **50**, 957 (2018).

[5] H. D. Young, R. A. Freedman, and A. L. Ford, *University Physics with Modern Physics*, 16th ed. (Pearson, San Francisco, 2023).

[6] Australian Radiation Protection and Nuclear Safety Agency, "Gamma radiation," (2024), accessed: 2024-08-09.

[7] C. F. Bohren and D. R. Huffman, *Absorption and Scattering of Light by Small Particles* (Wiley-VCH, Weinheim, Germany, 2004).

[8] International Atomic Energy Agency, *Radiation Protection and Safety of Radiation Sources: International Basic Safety Standards*, IAEA Safety Standards Series No. GSR Part 3 (IAEA, Vienna, Austria, 2024).

[9] H. Cember and T. E. Johnson, *Introduction to Health Physics*, 4th ed. (McGraw-Hill Medical, New York, NY, 2008).

[10] K. S. Krane, *Gamma and X-ray spectrometry with semiconductor detectors* (Springer Science & Business Media, 1987).

[11] J. A. Smith and J. D. Brown, J. Med. Phys. **25**, 123 (2000).

[12] B. Aygün, Nucl. Eng. Technol. **52**, 647 (2020).

[13] C. Perrier and E. Segrè, Nat. **140**, 193 (1937).

[14] R. Johnson and L. Wang, Health Phys. **89**, 123 (2005).

[15] H. Ebendorff-Heidepriem and D. Ehrt, Opt. Mater. **19**, 351 (2002).

[16] K. S. Mann, M. S. Heer, and A. Rani, Appl. Clay Sci. **119**, 249 (2016).

[17] J. E. Martin and S. L. Thompson, J. Radiat. Res. **43**, 123 (2002).

[18] A. Einstein, Ann. Phys. **17**, 132 (1905).

[19] D. Coomber, *Radiochemical Methods in Analysis* (Springer Science & Business Media, 2012).

[20] M. Iqbal, *An Introduction to Solar Radiation* (Elsevier, 2012).

[21] D. Chaney and J. Harris, Phys. Rep. **489**, 149 (2009).

[22] K. S. Krane, *Introductory Nuclear Physics* (John Wiley & Sons, 1991).

[23] S. Kahn and M. E. Jones, Rev. Mod. Phys. **93**, 025003 (2021).

[24] J. W. Gofman, *Radiation and Human Health* (Sierra Club Books, San Francisco, CA, 1981).

[25] F. H. Attix, *Introduction to Radiological Physics and Radiation Dosimetry* (John Wiley & Sons, 2008).

[26] H. W. Koch and J. W. Motz, Rev. Mod. Phys. **31**, 920 (1959).

[27] E. McGuire, Phys. Rev. A **57**, 2758 (1998).

[28] S. S. Obaid, D. K. Gaikwad, and P. P. Pawar, Radiat. Phys. Chem. **144**, 356 (2018).

[29] I. Olarinoye, F. El-Agawany, A. El-Adawy, Y. Rammah, *et al.*, Ceram. Int. **46**, 23134 (2020).

[30] S. Akbulut, A. Sehhatigdiri, H. Eroglu, and S. Çelik, Radiat. Phys. Chem. **117**, 88 (2015).

[31] T. Van Thuong, O. Tashlykov, and K. Mahmoud, Nucl. Eng. Technol. **56**, 666 (2024).

[32] D. K. Nzivulu, N. O. Hashim, N. Musila, K. E. Otieno, and F. O. Wanjala, MethodsX **12**, 102744 (2024).

[33] R. A. Bantan, M. Sayyed, K. Mahmoud, and Y. Al-Hadeethi, Prog. Nucl. Energy **126**, 103405 (2020).

[34] M. Sayyed, M. AlZaatreh, M. Dong, M. Zaid, K. Matori, and H. Tekin, Results Phys. **7**, 2528 (2017).

[35] A. Dulal, D. R. Upadhyay, S. M. Tajudin, and R. Khanal, Mater. Res. Express **11**, 075202 (2024).

[36] A. A. El-Sawy and E. Sarwat, Baghdad Sci. J. **21**, 0480 (2024).

[37] M. Sayyed, U. Rilwan, K. Mahmoud, and M. Elsafi, Nucl. Eng. Technol. **56**, 2437 (2024).

[38] I. Olarinoye, S. Alomairy, C. Sriwunkum, and M. S. Al-Buriahi, Phys. Scr. **96**, 065308 (2021).

[39] H. S. Mann, G. S. Brar, K. S. Mann, and G. S. Mudahar, Nucl. Eng. Technol. **48**, 1230 (2016).

[40] S.-C. Kim and S.-H. Cho, Appl. Sci. **9**, 1765 (2019).

[41] M. N. Amin, I. Ahmad, A. Abbas, K. Khan, M. G. Qadir, M. Iqbal, A. M. Abu-Arab, and A. A. Alabdullah, Mater. **15**, 5908 (2022).

[42] C. Douvris, T. Vaughan, D. Bussan, G. Bartzas, and R. Thomas, Sci. Total Environ. **905**, 167242 (2023).

[43] C. Hall and A. Hamilton, Mater. Struct. **49**, 3969 (2016).

[44] Y. Watanabe, Phys. Med. Biol. **44**, 2201 (1999).

[45] H. Tekin and O. Kilicoglu, J. Alloys Compd. **815**, 152484 (2020).

[46] A. Abouhaswa, M. Al-Buriahi, M. Chalermpon, and Y. Rammah, Appl. Phys. A **126**, 1 (2020).

[47] S. Stalin, D. Gaikwad, M. Al-Buriahi, C. Srinivasu, S. A. Ahmed, H. Tekin, and S. Rahman, Ceram. Int. **47**, 5286 (2021).

[48] M. Halimah, A. Azuraida, M. Ishak, and L. Hasnimulyati, J. Non-Cryst. Solids **512**, 140 (2019).

[49] A. Levet, E. Kavaz, and Y. Özdemir, J. Alloys Compd. **819**, 152946 (2020).

[50] M. Sayyed, Can. J. Phys. **94**, 1133 (2016).

[51] E. Şakar, Ö. F. Özpolat, B. Alım, M. Sayyed, and M. Kurudirek, Radiat. Phys. Chem. **166**, 108496 (2020).

[52] T. Sato, Y. Iwamoto, S. Hashimoto, T. Ogawa, T. Furuta, S.-i. Abe, T. Kai, P.-E. Tsai, N. Matsuda, H. Iwase, *et al.*, J. Nucl. Sci. Technol. **55**, 684 (2018).

[53] D. R. Upadhyay, S. M. Tajudin, and R. Khanal, Ceram. Int. **49**, 23118 (2023).

[54] E. H. Sondheimer, Adv. Phys. **50**, 499 (2001).

[55] N. J. AbuAlRoos, N. A. B. Amin, and R. Zainon, Radiat. Phys. Chem. **165**, 108439 (2019).

[56] A. El-Khayatt, Ann. Nucl. Energy **37**, 218 (2010).

Appendices

Spectra given by Syngistix ICP Continous software employed in ICP-OES

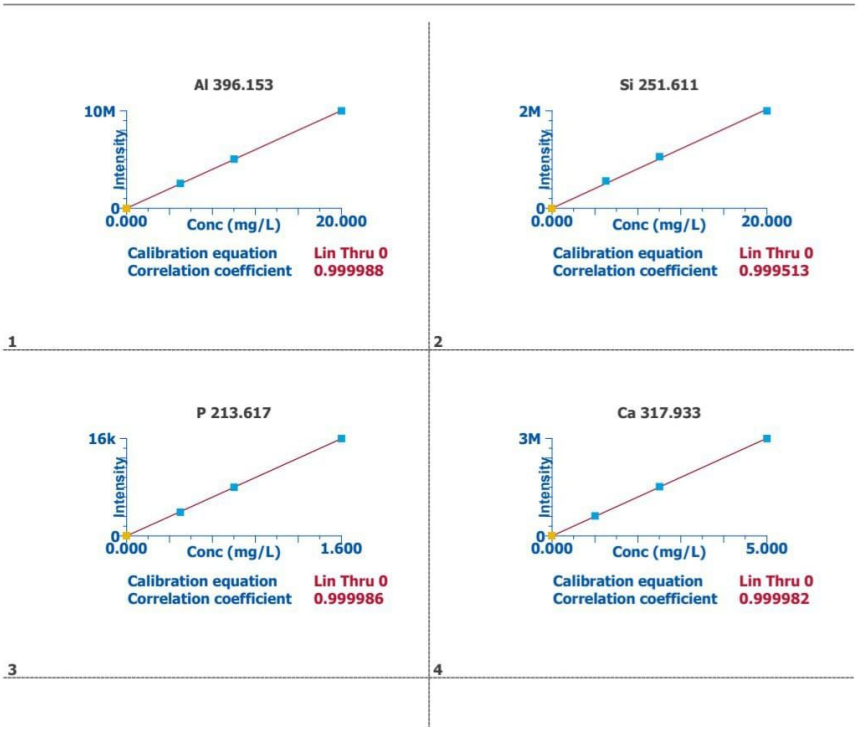

Figure 5.1: Calibration graph

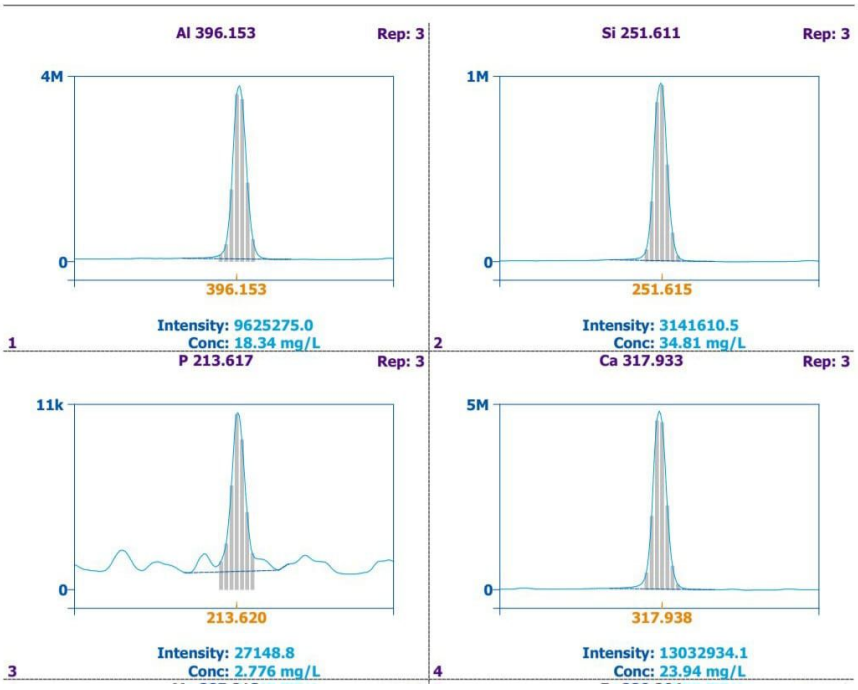

Figure 5.2: Calibration curve